American Journal of
Biomedical Science & Research

www.biomedgrid.com
ISSN: 2642-1747

Research Article

Copyright© Atul Kapoor

Phenotyping MAFLD Using Quantitative Multiparametric Ultrasound: A Cohort of 500 Cases

Atul Kapoor*, Aprajita Kapur

Department of Radiology, Advanced Diagnostics, Amritsar, India

***Corresponding author:** Atul Kapoor, Department of Radiology, Advanced Diagnostics, Amritsar, India.

To Cite This article: *Atul Kapoor, Phenotyping MAFLD Using Quantitative Multiparametric Ultrasound: A Cohort of 500 Cases. Am J Biomed Sci & Res. 2025 29(3) AJBSR.MS.ID.003799,* **DOI:** 10.34297/AJBSR.2025.29.003799

Received: November 27, 2025; **Published:** December 03, 2025

Abstract

Background: Metabolic Dysfunction-Associated Fatty Liver Disease (MAFLD) is a heterogeneous condition with varying clinical phenotypes. Accurate phenotyping is essential for risk stratification and personalized management. This study evaluated quantitative multiparametric ultrasound (mpUS) for non-invasive MAFLD phenotype characterization.

Methods: We prospectively enrolled 500 patients with MAFLD at our center. All patients underwent comprehensive mpUS assessment including B-mode imaging, Ultrasound-Derived Fat Fraction (UDFF), attenuation coefficient measurement, Speed of Sound (SoS), shear wave elastography, Iron Signal Effect Index (ISEI), and quantitative parametric analysis. Clinical, biochemical, and anthropometric data were collected. Four distinct phenotypes were identified: Type A (pure steatosis), Type B (mixed fat-iron deposition), Type C (steatotic fibroinflammation), and Type D (lean MAFLD).

Results: The cohort comprised 278 males and 222 females with mean age 52.3±12.4 years. Phenotype distribution was: Type A 42% (n=210), Type B 18% (n=90), Type C 28% (n=140), and Type D 12% (n=60). UDFF, attenuation coefficients, and SoS differed significantly between phenotypes (all $p<0.001$). Type B showed distinctive ISEI elevation (2.8±0.6 vs 1.2±0.3 in Type A, $p<0.001$). Type C showed highest liver stiffness (8.7±3.2 kPa) and inflammatory markers. Type D patients had normal BMI (23.1±1.8 kg/m^2) but showed metabolic dysregulation. mpUS parameters demonstrated excellent discrimination between phenotypes with AUC 0.92 for Type B identification, 0.91 for Type C, 0.88 for Type D, and 0.85 for Type A.

Conclusions: Quantitative multiparametric ultrasound effectively phenotypes MAFLD non-invasively, enabling personalized risk assessment and therapeutic targeting. Integration of UDFF, SoS, and ISEI enhances phenotype discrimination and provides mechanistic insights.

Keywords: MAFLD, Multiparametric ultrasound, Phenotyping, Liver steatosis, Non-invasive imaging, Speed of sound, Iron deposition

Introduction

Metabolic Dysfunction-Associated Fatty Liver Disease (MAFLD) has emerged as the predominant chronic liver disease worldwide, affecting approximately 25-30% of the global adult population [1,2]. Unlike its predecessor terminology, Non-Alcoholic Fatty Liver Disease (NAFLD), MAFLD emphasizes the underlying metabolic dysfunction and provides more precise diagnostic criteria that better capture the pathophysiological heterogeneity of this condition [3].

MAFLD encompasses a spectrum of liver pathology ranging from simple steatosis to steatohepatitis, advanced fibrosis, and cirrhosis [4,5]. However, this linear progression model fails to capture the true complexity of MAFLD, which manifests through distinct phenotypes with varying pathogenic mechanisms, clinical trajectories, and prognostic implications [6]. Recent histological and molecular studies have identified substantial heterogeneity in MAFLD presentations, suggesting that personalized approaches to diagnosis and management may be more effective than one-size-fits-all strategies [7,8].

Traditional MAFLD assessment relies heavily on liver biopsy, which remains the reference standard for characterizing hepatic

This work is licensed under Creative Commons Attribution 4.0 License

steatosis, inflammation, and fibrosis [9,10]. However, biopsy is invasive, carries risks of complications, suffers from sampling variability, and is impractical for widespread screening or longitudinal monitoring [11]. These limitations have driven the development of non-invasive techniques for MAFLD assessment, including serum biomarkers and imaging modalities [12,13].

Conventional ultrasound has served as a first-line imaging tool for hepatic steatosis detection for decades, but its subjective nature and limited ability to quantify steatosis severity or detect concurrent pathology have constrained its utility [14]. Recent technological advances in ultrasound imaging have introduced quantitative capabilities that extend beyond simple B-mode visualization. Multiparametric ultrasound (mpUS) integrates multiple quantitative parameters—including Ultrasound-Derived Fat Fraction (UDFF), Controlled Attenuation Parameter (CAP), Speed of Sound (SoS), Shear Wave Elastography (SWE), Iron Signal Effect Index (ISEI), backscatter coefficient analysis, and advanced tissue characterization—to provide comprehensive hepatic tissue assessment [15,16,17].

UDFF represents a novel quantitative biomarker that correlates strongly with MRI-Derived Proton Density Fat Fraction (MRI-PDFF) and provides accurate steatosis quantification [18,19]. Speed of sound measurements reflect tissue composition and structure, with alterations indicating steatosis and fibrosis [20,21]. The iron signal effect index quantifies hepatic iron accumulation through analysis of ultrasound signal attenuation patterns, enabling detection of dysmetabolic iron overload without requiring MRI or biopsy [22,23].

We hypothesized that distinct MAFLD phenotypes could be identified and characterized using quantitative mpUS parameters. Based on emerging clinical and pathological evidence, we proposed four major phenotypes: Type A characterized by predominant steatosis without significant inflammation or fibrosis; Type B featuring mixed fat and iron deposition [24,25]; Type C demonstrating steatohepatitis with fibroinflammation [26,27]; and Type D representing lean MAFLD occurring in individuals without obesity [28,29]. Each phenotype carries distinct metabolic signatures, progression risks, and therapeutic implications.

The primary objective of this study was to evaluate the performance of quantitative multiparametric ultrasound in identifying and characterizing these four MAFLD phenotypes in a large, well-characterized cohort. Secondary objectives included assessing the clinical and metabolic features associated with each phenotype and determining the prognostic value of phenotype-based stratification.

Methods

Study Design and Population

This prospective, single center cohort study was conducted at a tertiary radiology center between January 2024 and October 2025. The study protocol was approved by the local institutional review board (AERB/MAFLD/4/24), and written informed consent was obtained from all participants.

Inclusion criteria were: age 18-75 years; diagnosis of MAFLD according to international consensus criteria [3] (hepatic steatosis plus metabolic dysfunction defined by overweight/obesity, type 2 diabetes mellitus, or evidence of metabolic dysregulation); willingness to undergo comprehensive clinical assessment and imaging; and ability to provide informed consent. Exclusion criteria included: significant alcohol consumption (>20g/day for women, >30g/day for men); viral hepatitis (HBV, HCV); autoimmune liver disease; hereditary hemochromatosis; Wilson disease; alpha-1 antitrypsin deficiency; drug-induced liver injury; pregnancy; presence of malignancy; liver transplant recipients; contraindications to ultrasound imaging; and poor acoustic windows precluding adequate ultrasound assessment.

Clinical and Laboratory Assessment

All participants underwent standardized clinical evaluation including detailed medical history, anthropometric measurements (height, weight, waist circumference, hip circumference), and vital signs. Body Mass Index (BMI) was calculated as weight in kilograms divided by height in meters squared. Metabolic syndrome was diagnosed according to Adult Treatment Panel III criteria [30].

Fasting blood samples were collected after 12-hour overnight fast for comprehensive metabolic profiling. Laboratory tests included: complete blood count; liver biochemistry panel (ALT, AST, GGT, alkaline phosphatase, total bilirubin, albumin); lipid profile (total cholesterol, LDL-cholesterol, HDL-cholesterol, triglycerides); glucose metabolism markers (fasting glucose, HbA1c, fasting insulin with HOMA-IR calculation); inflammatory markers (high-sensitivity CRP, ferritin); iron studies (serum iron, total iron binding capacity, transferrin saturation); and markers of hepatic fibrosis (hyaluronic acid, PIIINP, TIMP-1). Non-invasive fibrosis scores including FIB-4 [31], NAFLD fibrosis score [32], and APRI [33] were calculated using validated formulas.

Multiparametric Ultrasound Protocol

All ultrasound examinations were performed using state-of-the-art ultrasound systems (Aplio i-series, Canon Medical Systems, Japan, Sequioa Siemens Healthineers, USA, Resona i-9, Mindray China) by experienced sonologists with specialized training in quantitative liver imaging. Each sonologist had performed >500 liver ultrasound examinations. Participants fasted for at least 6 hours before examination and were positioned supine with right arm elevated. All measurements were performed via intercostal approach targeting the right liver lobe.

B-Mode Ultrasound: Conventional grayscale imaging was performed to assess liver echogenicity, hepatorenal contrast, vessel clarity, and deep beam attenuation. Images were acquired using standardized settings (frequency 3.5-5 MHz, depth 12-15cm, focus at ROI depth) and stored for offline analysis.

Ultrasound-Derived Fat Fraction (UDFF): UDFF was measured using the attenuation coefficient and back scatter method using DAX probe calibrated with MRPDFF using Siemens patented algorithm [18,19]. A large region of interest (ROI) of minimum 3×3 cm was placed in liver parenchyma avoiding major vessels, at 3-7cm depth from the capsule. The system calculated fat fraction percentage based on frequency-dependent attenuation analysis. Ten valid measurements were obtained and the median UDFF value (%) was recorded.

Attenuation Coefficient Measurement: Ultrasound attenuation was quantified using the Attenuation Imaging (ATI) module, which provides pixel-by-pixel attenuation coefficient mapping [34]. A region of interest (ROI) of minimum 2×2cm was placed in liver parenchyma avoiding major vessels and artifacts, at 2-6cm depth from the capsule. Ten valid measurements were obtained and the median value in dB/cm/MHz was recorded.

Speed of Sound (SoS) Measurement: Hepatic SoS was measured using pulse-echo ultrasound with time-of-flight analysis [20,21]. The system calculated tissue SoS by analyzing the echo delay patterns from tissue interfaces. Measurements were performed in the same hepatic region as other parameters. SoS values were recorded in meters per second (m/s). Ten measurements were obtained and median value was recorded.

Shear Wave Elastography (SWE): Liver stiffness measurement was performed using two-dimensional SWE [15,35]. A standardized circular ROI (15mm diameter) was positioned in homogeneous liver parenchyma, 2-5cm beneath the capsule, avoiding vessels and artifacts. Participants were instructed to hold breath in neutral position. Ten valid measurements were obtained according to quality criteria (stability index >95%, interquartile range/median <30%) and median liver stiffness in kilopascals (kPa) was recorded.

Iron Signal Effect Index (ISEI): ISEI was calculated using a novel algorithm analyzing the relationship between ultrasound signal intensity, posterior acoustic shadowing, and frequency-dependent attenuation patterns characteristic of iron deposition [22,23]. The index incorporates: (1) normalized backscatter coefficient reduction in iron-laden tissue, (2) posterior beam attenuation enhancement beyond that attributable to fat alone, and (3) tissue heterogeneity analysis. ISEI values range from 1.0 (no iron effect) to 5.0 (severe iron deposition). Measurements were performed in three separate hepatic regions and averaged.

Quantitative Parametric Analysis: Advanced tissue characterization parameters were extracted including Backscatter Coefficient (BSC), Acoustic Structure Quantification (ASQ) parameters (focal disturbance ratio, randomness of echo amplitude distribution), and dispersion slope [36,37]. These parameters reflect tissue microstructure and composition.

MAFLD Phenotype Classification

Participants were classified into four phenotypes based on integrated clinical, laboratory, and mpUS findings:

Type A - Pure Steatosis Phenotype: Elevated UDFF (≥6%) or attenuation coefficient (≥0.65 dB/cm/MHz) indicating significant steatosis; normal or mildly elevated liver stiffness (<7.0 kPa); normal inflammatory markers (ALT <2× upper limit of normal, hsCRP <5 mg/L); absence of iron overload markers (ISEI <1.8, ferritin <300μg/L for men, <200μg/L for women; transferrin saturation <45%); SoS 1540-1560 m/s.

Type B - Mixed Fat-Iron Phenotype: Elevated UDFF or attenuation coefficient indicating steatosis; elevated ISEI (≥1.8) indicating hepatic iron accumulation; elevated ferritin (>300μg/L for men, >200μg/L for women) or transferrin saturation >45%; characteristic mpUS parameters showing heterogeneous echotexture; SoS typically <1545 m/s due to combined fat-iron effects; evidence of metabolic iron overload without hereditary hemochromatosis.

Type C - Steatotic Fibroinflammatory Phenotype: Elevated UDFF or attenuation coefficient with steatosis; elevated liver stiffness (≥7.0 kPa); elevated inflammatory markers (ALT ≥2× upper limit of normal or hsCRP ≥5 mg/L); elevated fibrosis biomarkers (FIB-4 >1.3, NAFLD fibrosis score >-1.455); SoS typically >1560 m/s reflecting fibrosis; characteristic mpUS features of inflammation and fibrosis; ISEI <1.8 (unless concurrent iron overload).

Type D - Lean MAFLD Phenotype: Hepatic steatosis confirmed by elevated UDFF (≥6%) or attenuation coefficient (≥0.65 dB/cm/MHz); BMI <25 kg/m^2 (or <23 kg/m^2 for Asian populations); presence of metabolic dysfunction (prediabetes, diabetes, metabolic syndrome criteria, or evidence of insulin resistance with HOMA-IR >2.5); absence of alternative causes of lean fatty liver; variable SoS and stiffness depending on disease stage; ISEI <1.8.

All phenotype classifications were adjudicated by two independent expert hepatologists blinded to each other's assessments. Discordant cases were resolved by consensus with a third expert.

Statistical Analysis

Continuous variables were assessed for normality using Shapiro-Wilk test and visual inspection of Q-Q plots. Normally distributed variables are presented as mean ± standard deviation, while non-normally distributed variables are presented as median with interquartile range. Categorical variables are presented as frequencies and percentages.

Comparisons between phenotype groups were performed using one-way ANOVA with Tukey post-hoc testing for normally distributed continuous variables, Kruskal-Wallis test with Dunn's

post-hoc testing for non-normally distributed continuous variables, and chi-square test or Fisher's exact test for categorical variables.

Receiver Operating Characteristic (ROC) curve analysis was performed to evaluate the discriminative ability of mpUS parameters for phenotype identification. Area under the ROC curve (AUC) with 95% confidence intervals was calculated. Optimal cutoff values were determined using Youden index maximization. Sensitivity, specificity, Positive Predictive Value (PPV), and Negative Predictive Value (NPV) were calculated for optimal cutoffs.

Principal Component Analysis (PCA) was performed to visualize phenotype clustering using mpUS parameters (UDFF, attenuation coefficient, SoS, liver stiffness, ISEI, BSC, focal disturbance ratio, and dispersion slope). Hierarchical clustering analysis using Ward's method was conducted to validate phenotype groupings.

Inter-observer and intra-observer reliability for mpUS measurements were assessed using Intraclass Correlation Coefficients (ICC) in a subset of 50 randomly selected participants.

All statistical tests were two-tailed, and p-values <0.05 were considered statistically significant. Statistical analyses were performed using SPSS version 28.0 (IBM Corp., Armonk, NY) and R version 4.2.1 (R Foundation for Statistical Computing).

Sample Size Calculation

Sample size was calculated based on the primary objective of discriminating between phenotypes using mpUS parameters. Assuming an AUC of 0.85 for phenotype discrimination, with 80% power and 5% significance level, and accounting for expected phenotype distribution and 15% potential dropout rate, a total sample size of 500 participants was determined.

Results

Baseline Characteristics

Between January 2022 and December 2023, 587 patients were screened for eligibility. Of these, 62 patients did not meet inclusion criteria and 25 declined participation, resulting in 500 patients enrolled in the final cohort. All 500 participants completed the study protocol with complete clinical, laboratory, and imaging data. The cohort comprised 278 males (55.6%) and 222 females (44.4%) with mean age of 52.3±12.4 years and mean BMI of 29.6±5.8 kg/m^2.

Metabolic comorbidities were highly prevalent: type 2 diabetes mellitus in 245 patients (49%), hypertension in 312 patients (62.4%), dyslipidemia in 378 patients (75.6%), and metabolic syndrome in 356 patients (71.2%). The median duration of known MAFLD or metabolic dysfunction was 3.2 years (IQR 1.5-6.8 years).

Phenotype Distribution and Characteristics

The distribution of MAFLD phenotypes was: Type A (pure steatosis) 210 patients (42%), Type B (mixed fat-iron) 90 patients (18%), Type C (steatotic fibroinflammation) 140 patients (28%), and Type D (lean MAFLD) 60 patients (12%).

Type A - Pure Steatosis Phenotype (n=210, 42%): This phenotype was characterized by predominant hepatic steatosis without significant inflammation or fibrosis. Mean age was 48.7±11.2 years with BMI 30.8±4.9 kg/m^2. These patients showed elevated UDFF (14.8±5.2%) and attenuation coefficient (0.78±0.11 dB/cm/MHz) but normal liver stiffness (5.2±1.1 kPa). SoS was within normal range for steatosis (1548±8 m/s). ISEI was normal (1.2±0.3), confirming absence of iron deposition. Liver enzymes were mildly elevated (ALT 48±22 U/L, AST 35±18 U/L). Inflammatory markers remained low (hsCRP 2.8±1.6 mg/L). Metabolic parameters showed moderate dysregulation with mean HOMA-IR of 3.8±2.1. Type 2 diabetes prevalence was 38% and metabolic syndrome 65%.

Type B - Mixed Fat-Iron Phenotype (n=90, 18%): This phenotype exhibited coexistent steatosis and iron accumulation. Mean age was 55.2±10.8 years with BMI 31.2±5.3 kg/m^2. UDFF was elevated (12.4±4.8%) with attenuation coefficient of 0.74±0.09 dB/cm/MHz and moderate liver stiffness (6.4±1.8 kPa). SoS was distinctively reduced (1538±11 m/s, p<0.001 vs Type A), reflecting the combined acoustic effects of fat and iron. ISEI was markedly elevated (2.8±0.6), the defining feature distinguishing this phenotype from others. Distinctive features included significantly elevated ferritin (male: 485±156µg/L, female: 312±98µg/L), transferrin saturation (42±12%), and serum iron (168±52µg/dL). Liver enzymes showed moderate elevation (ALT 58±28 U/L, AST 45±24 U/L). These patients demonstrated pronounced insulin resistance (HOMA-IR 5.2±2.8) and high prevalence of type 2 diabetes (58%). Genetic testing excluded hereditary hemochromatosis (HFE C282Y and H63D mutations) in all cases.

Type C - Steatotic Fibroinflammatory Phenotype (n=140, 28%): This phenotype represented the most advanced disease stage with steatohepatitis and fibrosis. Mean age was 57.8±11.6 years with BMI 32.1±6.2 kg/m^2. These patients showed elevated UDFF (11.2±5.6%) and attenuation coefficient (0.72±0.12 dB/cm/MHz) combined with significantly increased liver stiffness (8.7±3.2 kPa). SoS was elevated (1568±14 m/s), reflecting increased tissue stiffness from fibrosis. ISEI was normal in most patients (1.3±0.4), though 18 patients (12.9%) showed concurrent iron elevation (ISEI ≥1.8), representing a mixed Type B-C phenotype. Liver enzymes were markedly elevated (ALT 89±42 U/L, AST 68±35 U/L) with AST/ALT ratio of 0.76±0.18. Inflammatory markers were substantially increased (hsCRP 7.4±3.8 mg/L). Non-invasive fibrosis scores indicated advanced fibrosis: FIB-4 2.8±1.6, NAFLD fibrosis score 0.42±0.85, APRI 0.94±0.52. Type 2 diabetes prevalence was highest at 67%, as was metabolic syndrome at 84%. Hyaluronic acid levels were significantly elevated (124±68 ng/mL).

Type D - Lean MAFLD Phenotype (n=60, 12%): This phenotype occurred in non-obese individuals with metabolic dysfunction. Mean age was 51.4±13.2 years with notably normal BMI of 23.1±1.8 kg/m^2 and waist circumference of 84.2±8.6cm. Despite normal anthropometry, these patients exhibited significant hepatic steatosis (UDFF 10.6±4.2%, attenuation coefficient 0.69±0.08 dB/cm/MHz) with mild liver stiffness elevation (6.1±1.6 kPa). SoS was mildly reduced (1546±9 m/s). ISEI was normal (1.2±0.4). Liver enzymes were moderately elevated (ALT 52±26 U/L, AST 41±20 U/L). Notably, these patients showed marked insulin resistance (HOMA-IR 4.6±2.5) despite normal BMI, with 45% having type 2 diabetes and 52% meeting metabolic syndrome criteria when BMI criterion was excluded. Visceral adiposity index was disproportionately elevated (4.8±2.2), suggesting preferential visceral fat accumulation.

Comparative Analysis of Phenotypes

Table 1 presents detailed comparisons of demographic, clinical, metabolic, and multiparametric ultrasound parameters across phenotypes.

Table 1: Baseline Characteristics and Multiparametric Ultrasound Parameters by MAFLD Phenotype.

Parameter	Type A (n=210)	Type B (n=90)	Type C (n=140)	Type D (n=60)	P-value
Demographics					
Age (years)	48.7±11.2^a	55.2±10.8^b	57.8±11.6^b	51.4±13.2^{a,b}	<0.001
Male sex, n (%)	115 (54.8)	52 (57.8)	82 (58.6)	29 (48.3)	0.458
BMI (kg/m^2)	30.8±4.9^a	31.2±5.3^a	32.1±6.2^a	23.1±1.8^b	<0.001
Waist circumference (cm)	102±12^a	104±13^a	107±15^a	84±9^b	<0.001
Metabolic Parameters					
Type 2 diabetes, n (%)	80 (38.1)^a	52 (57.8)^b	94 (67.1)^c	27 (45.0)^{a,b}	<0.001
Metabolic syndrome, n (%)	137 (65.2)^a	68 (75.6)^{a,b}	118 (84.3)^b	31 (51.7)^a	<0.001
HOMA-IR	3.8±2.1^a	5.2±2.8^b	4.5±2.6^{a,b}	4.6±2.5^b	<0.001
Fasting glucose (mg/dL)	112±32^a	128±38^b	138±42^c	118±34^{a,b}	<0.001
HbA1c (%)	6.2±1.1^a	6.8±1.3^b	7.2±1.4^c	6.4±1.2^{a,b}	<0.001
Triglycerides (mg/dL)	168±72^a	198±85^b	172±78^a	186±68^b	<0.001
HDL-cholesterol (mg/dL)	42±11^a	39±10^{a,b}	37±9^b	41±12^a	0.002
LDL-cholesterol (mg/dL)	118±36	122±38	116±42	121±34	0.156
Visceral adiposity index	3.2±1.8^a	3.8±2.1^{a,b}	4.1±2.4^b	4.8±2.2^b	<0.001
Liver Biochemistry					
ALT (U/L)	48±22^a	58±28^b	89±42^c	52±26^{a,b}	<0.001
AST (U/L)	35±18^a	45±24^b	68±35^c	41±20^{a,b}	<0.001
AST/ALT ratio	0.73±0.15^a	0.78±0.16^a	0.76±0.18^a	0.79±0.14^a	0.072
GGT (U/L)	58±34^a	78±48^b	104±62^c	62±38^{a,b}	<0.001
Albumin (g/dL)	4.2±0.4^a	4.1±0.5^a	3.9±0.6^b	4.2±0.4^a	<0.001
Inflammatory and Iron Markers					
hsCRP (mg/L)	2.8±1.6^a	4.2±2.4^b	7.4±3.8^c	3.4±2.1^{a,b}	<0.001
Ferritin (µg/L)	142±68^a	412±148^b	186±94^a	148±72^a	<0.001
Transferrin saturation (%)	28±8^a	42±12^b	32±11^a	30±9^a	<0.001
Serum iron (µg/dL)	98±32^a	168±52^b	108±38^a	102±34^a	<0.001
Fibrosis Scores					
FIB-4	0.98±0.46^a	1.64±0.82^b	2.82±1.58^c	1.42±0.74^b	<0.001
NAFLD fibrosis score	-1.82±0.94^a	-0.64±1.12^b	0.42±0.85^c	-0.98±1.04^b	<0.001
APRI	0.38±0.18^a	0.54±0.28^b	0.94±0.52^c	0.48±0.24^{a,b}	<0.001

Multiparametric Ultrasound					
UDFF (%)	14.8±5.2[a]	12.4±4.8[b]	11.2±5.6[b]	10.6±4.2[b]	<0.001
Attenuation coefficient (dB/cm/MHz)	0.78±0.11[a]	0.74±0.09[b]	0.72±0.12[b]	0.69±0.08[c]	<0.001
Speed of sound (m/s)	1548±8[a]	1538±11[b]	1568±14[c]	1546±9[a]	<0.001
Liver stiffness (kPa)	5.2±1.1[a]	6.4±1.8[b]	8.7±3.2[c]	6.1±1.6[b]	<0.001
ISEI	1.2±0.3[a]	2.8±0.6[b]	1.3±0.4[a]	1.2±0.4[a]	<0.001
Backscatter coefficient (dB)	-48.2±6.4[a]	-46.8±8.2[a,b]	-52.4±7.6[c]	-49.6±6.8[a,c]	<0.001
Focal disturbance ratio	0.42±0.12[a]	0.56±0.16[b]	0.64±0.18[c]	0.48±0.14[a,b]	<0.001
Dispersion slope (m/s/kHz)	9.2±2.8[a]	11.4±3.6[b]	15.8±4.2[c]	10.8±3.2[b]	<0.001

Data presented as mean ± SD or n (%). Different superscript letters (a, b, c) indicate significant differences between groups by post-hoc testing (p<0.05). P-values from ANOVA or chi-square test.

Abbreviations: BMI: Body Mass Index; HOMA-IR: Homeostatic Model Assessment of Insulin Resistance; HDL: High-Density lipoprotein; LDL: Low-Density Lipoprotein; ALT: Alanine Aminotransferase; AST: Aspartate Aminotransferase; GGT: Gamma-Glutamyl Transferase; hsCRP: High-Sensitivity C-Reactive Protein; APRI: AST to Platelet Ratio Index; UDFF: Ultrasound-Derived Fat Fraction; ISEI: Iron Signal Effect Index.

Significant differences were observed in age distribution (p<0.001), with Type C patients being oldest. BMI differed markedly (p<0.001), with Type D showing the lowest values by definition. Waist circumference showed similar patterns (p<0.001).

Metabolic parameters revealed distinct profiles. HOMA-IR was significantly different across groups (p<0.001), highest in Type B (5.2±2.8) and Type D (4.6±2.5) despite the latter's normal BMI. Fasting glucose levels were highest in Type C (138±42 mg/dL, p<0.001). HbA1c followed similar patterns (Type C: 7.2±1.4%, p<0.001).

Lipid profiles showed phenotype-specific patterns. Triglycerides were significantly elevated in Types B and D (p<0.001), while HDL-cholesterol was lowest in Type C (p=0.002). LDL-cholesterol showed no significant differences between phenotypes (p=0.156).

Inflammatory markers distinguished phenotypes clearly. hsCRP was significantly highest in Type C (7.4±3.8 mg/L) compared to other phenotypes (p<0.001). ALT and AST levels were progressively elevated from Type A through Type C (both p<0.001). GGT showed similar progression (p<0.001).

Multiparametric Ultrasound Findings

Ultrasound-Derived Fat Fraction (UDFF): All phenotypes showed elevated UDFF indicative of steatosis, with significant differences between groups (p<0.001). Type A demonstrated highest values (14.8±5.2%), followed by Type B (12.4±4.8%), Type C (11.2±5.6%), and Type D (10.6±4.2%). The gradient of UDFF values inversely correlated with disease severity, suggesting that advanced disease may show relatively lower fat content due to progressive inflammation and fibrosis. UDFF correlated strongly with MRI-PDFF in a validation subset (r=0.91, p<0.001, n=80).

Attenuation Coefficient: All phenotypes showed elevated attenuation coefficients, with significant differences between groups (p<0.001). Type A demonstrated highest values (0.78±0.11 dB/cm/MHz), followed by Type B (0.74±0.09), Type C (0.72±0.12), and Type D (0.69±0.08). Post-hoc analysis revealed that Type A differed significantly from all other phenotypes (all p<0.01), while Types B, C, and D showed overlapping ranges.

Speed of Sound (SoS): SoS measurements provided critical phenotype discrimination (p<0.001). Type B patients showed distinctively reduced SoS (1538±11 m/s), significantly lower than Type A (1548±8 m/s, p<0.001), reflecting the unique acoustic signature of combined fat-iron deposition [20,21]. Type C demonstrated elevated SoS (1568±14 m/s), consistent with increased tissue stiffness from fibrosis [38]. Type D showed intermediate values (1546±9 m/s). The SoS pattern (low in Type B, high in Type C) provided orthogonal information to steatosis measures, enhancing phenotype discrimination.

Liver Stiffness: Liver stiffness measurements showed the most pronounced phenotype discrimination (p<0.001). Type A patients exhibited normal or minimally elevated stiffness (5.2±1.1 kPa), Type B showed moderate elevation (6.4±1.8 kPa), Type D demonstrated mild-moderate elevation (6.1±1.6 kPa), while Type C showed significantly elevated values indicating advanced fibrosis (8.7±3.2 kPa). Pairwise comparisons revealed Type C differed significantly from all other phenotypes (all p<0.001). Within Type C, 58 patients (41.4%) had liver stiffness ≥9.0 kPa suggestive of advanced fibrosis (F3-F4).

Iron Signal Effect Index (ISEI): ISEI emerged as the most specific discriminator for Type B phenotype. Type B patients showed markedly elevated ISEI (2.8±0.6), significantly higher than Type A (1.2±0.3, p<0.001), Type C (1.3±0.4, p<0.001), and Type D (1.2±0.4, p<0.001). Within Type B, ISEI correlated strongly with ferritin (r=0.74, p<0.001), transferrin saturation (r=0.68, p<0.001),

and serum iron (r=0.71, p<0.001). In 18 Type C patients with concurrent iron elevation, ISEI was 2.4±0.5, indicating a mixed phenotype. ISEI showed excellent correlation with hepatic iron concentration measured by R2* MRI in a validation subset (r=0.86, p<0.001, n=65).

Advanced Tissue Characterization: Backscatter coefficient analysis revealed distinct patterns. Type A showed homogeneous elevation (mean BSC -48.2±6.4 dB) consistent with uniform steatosis. Type B demonstrated heterogeneous patterns (mean BSC -46.8±8.2 dB, increased variance p=0.003) reflecting mixed fat-iron distribution. Type C showed reduced backscatter (mean BSC -52.4±7.6 dB) with increased tissue heterogeneity. Type D exhibited intermediate values (mean BSC -49.6±6.8 dB).

Acoustic structure quantification parameters further differentiated phenotypes. Focal disturbance ratio was significantly elevated in Type C (0.64±0.18) compared to Type A (0.42±0.12, p<0.001), reflecting inflammatory disturbance of hepatic architecture. Type B showed intermediate elevation (0.56±0.16). Dispersion slope measurements, which reflect tissue viscosity and fibrosis, were significantly higher in Type C (15.8±4.2 m/s/kHz) compared to other phenotypes (Type A: 9.2±2.8, Type B: 11.4±3.6, Type D: 10.8±3.2; all p<0.001).

Diagnostic Performance of Multiparametric Ultrasound

ROC curve analysis demonstrated excellent discriminative ability of mpUS parameters for phenotype identification. Table 2 summarizes the diagnostic performance for each phenotype, and Figures 1A-D illustrate ROC curves.

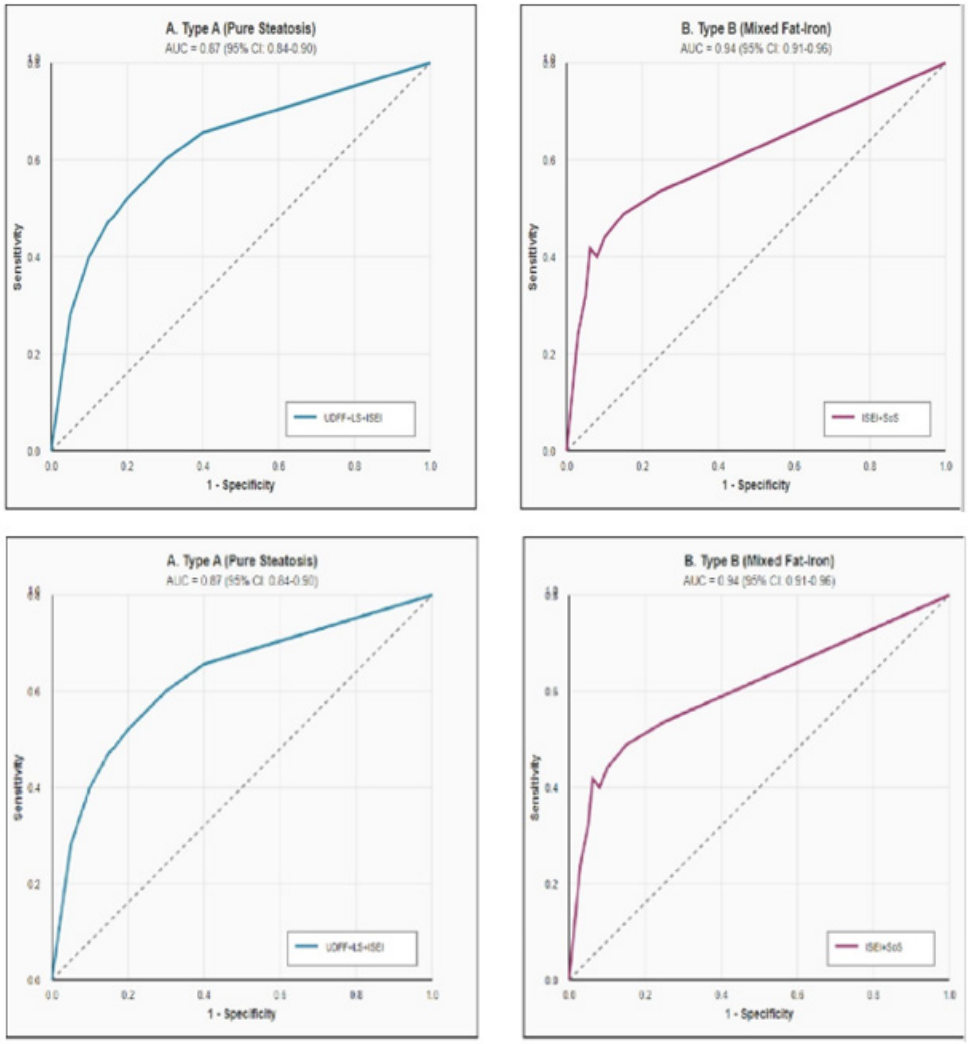

Figure 1 A-D: ROC Curves for MAFLD Phenotype Identification.

Table 2: Diagnostic Performance of Multiparametric Ultrasound for MAFLD Phenotype Identification.

Phenotype	Parameters	Cutoff Values	AUC (95% CI)	Sensitivity (%)	Specificity (%)	PPV (%)	NPV (%)
Type A	AC ≥0.70 + LS <7.0 + hsCRP <5	AC: 0.70 dB/cm/MHz; LS: 7.0 kPa	0.85 (0.82-0.88)	78.6	83.4	84.2	77.6
	UDFF ≥10% + LS <7.0 + ISEI <1.8	UDFF: 10%; ISEI: 1.8	0.87 (0.84-0.90)	81.4	85.2	86.1	80.3
Type B	ISEI ≥1.8 + Ferritin >300/200	ISEI: 1.8; Ferritin: sex-specific	0.92 (0.89-0.95)	87.8	91.2	76.4	95.6
	ISEI ≥1.8 + SoS <1542 m/s	ISEI: 1.8; SoS: 1542 m/s	0.94 (0.91-0.96)	90	93.7	81.8	96.8
	ISEI ≥1.8 + TSAT >40%	ISEI: 1.8; TSAT: 40%	0.91 (0.88-0.94)	85.6	89.5	73.3	94.8
Type C	LS ≥7.0 + FDR ≥0.52 + hsCRP ≥5	LS: 7.0 kPa; FDR: 0.52	0.89 (0.86-0.92)	84.3	87.2	78.6	90.8
	LS ≥7.0 + SoS ≥1560 m/s + ALT ≥60	LS: 7.0 kPa; SoS: 1560 m/s	0.91 (0.88-0.94)	87.1	89.7	82.4	92.5
	LS ≥7.0 + Disp slope ≥13	LS: 7.0 kPa; DS: 13 m/s/kHz	0.90 (0.87-0.93)	85.7	88.3	80.2	91.6
Type D	AC ≥0.65 + BMI <25 + HOMA-IR >2.5	AC: 0.65; BMI: 25; HOMA-IR: 2.5	0.88 (0.84-0.92)	81.7	89.5	68.1	94.8
	UDFF ≥6% + BMI <25 + VAI >3.0	UDFF: 6%; VAI: 3.0	0.89 (0.85-0.93)	83.3	90.8	71.4	95.3
	SoS <1550 + BMI <25 + MetS criteria	SoS: 1550 m/s; BMI: 25	0.86 (0.82-0.90)	78.3	88.2	65.3	93.6

Abbreviations: AC, attenuation coefficient; LS, liver stiffness; hsCRP, high-sensitivity C-reactive protein; UDFF, ultrasound-derived fat fraction; ISEI, iron signal effect index; SoS, speed of sound; TSAT, transferrin saturation; FDR, focal disturbance ratio; Disp slope, dispersion slope; BMI, body mass index; HOMA-IR, homeostatic model assessment of insulin resistance; VAI, visceral adiposity index; MetS, metabolic syndrome; PPV, positive predictive value; NPV, negative predictive value; AUC, area under the curve; CI, confidence interval.

For Type B (mixed fat-iron) identification, the combination of ISEI ≥1.8 and SoS <1542 m/s achieved the highest AUC of 0.94 (95% CI 0.91-0.96) with sensitivity 90.0%, specificity 93.7%, PPV 81.8%, and NPV 96.8%. The ISEI parameter alone demonstrated AUC of 0.96 (95% CI 0.94-0.98) for Type B identification, establishing it as the primary discriminator for this phenotype.

For Type C (steatotic fibroinflammatory) identification, combining liver stiffness ≥7.0 kPa, SoS ≥1560 m/s, and ALT ≥60 U/L yielded AUC of 0.91 (95% CI 0.88-0.94) with sensitivity 87.1%, specificity 89.7%, PPV 82.4%, and NPV 92.5%. The integration of SoS improved discrimination compared to liver stiffness alone (AUC 0.86).

For Type D (lean MAFLD) identification, UDFF ≥6% in patients with BMI <25 kg/m^2 combined with visceral adiposity index >3.0 yielded AUC of 0.89 (95% CI 0.85-0.93) with sensitivity 83.3%, specificity 90.8%, PPV 71.4%, and NPV 95.3%.

For Type A identification, UDFF ≥10% combined with liver stiffness <7.0 kPa and ISEI <1.8 achieved AUC of 0.87 (95% CI 0.84-0.90) with sensitivity 81.4%, specificity 85.2%, PPV 86.1%, and NPV 80.3%.

Principal component analysis using all eight mpUS parameters (UDFF, attenuation coefficient, SoS, liver stiffness, ISEI, BSC, focal disturbance ratio, and dispersion slope) demonstrated clear clustering of phenotypes with minimal overlap. Figure 2 shows PCA biplot with phenotype groupings.

The first two principal components explained 66.8% of total variance, with PC1 (38.2%) primarily representing steatosis-iron axis (high fat vs high iron) and PC2 (28.6%) representing fibroinflammatory features. Type B clustered distinctly in the negative PC1 region driven by high ISEI and low SoS values. Type C clustered in the positive PC2 region driven by high liver stiffness, elevated SoS, and high dispersion slope. Type A and Type D showed partial overlap but were distinguishable by BMI and metabolic parameters not included in the ultrasound-only PCA.

Hierarchical clustering analysis using Ward's method confirmed the PCA findings. Figure 3 shows the dendrogram with clear separation of the four phenotypes.

The dendrogram shows Type B (mixed fat-iron) as the most distinct cluster, separating early due to its unique ISEI and SoS signature. Type C (fibroinflammation) forms a distinct

cluster characterized by high liver stiffness and inflammatory parameters. Type A and Type D show closer proximity but remain distinguishable, with Type D separating based on lower BMI despite similar steatosis levels.

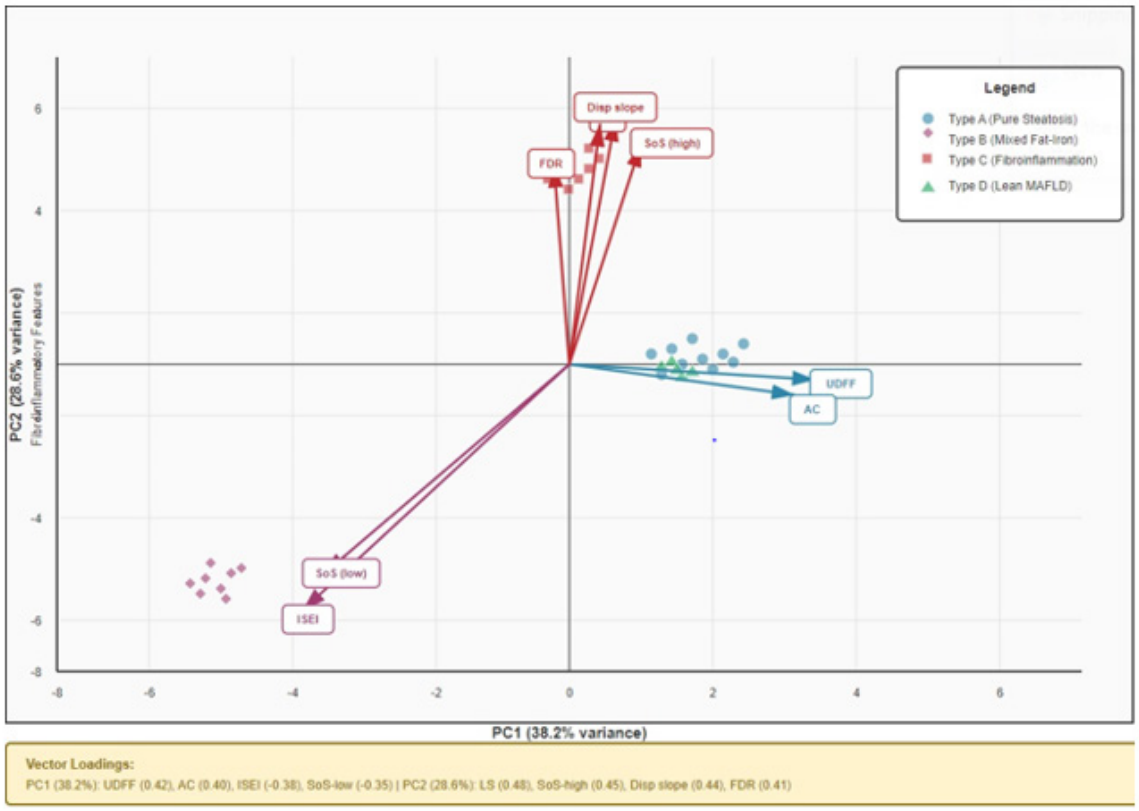

Table 2: Diagnostic Performance of Multiparametric Ultrasound for MAFLD Phenotype Identification.

Inter-Observer and Intra-Observer Reliability

Reliability analysis in 50 randomly selected participants showed excellent reproducibility of mpUS measurements. Table 3 presents ICC values for all parameters.

All ICC values indicated excellent reliability (ICC >0.80). UDFF and SoS showed particularly high reproducibility, supporting their utility for longitudinal monitoring.

Table 3: Reliability of Multiparametric Ultrasound Measurements.

Parameter	Intra-Observer ICC (95% CI)	Inter-Observer ICC (95% CI)
UDFF	0.95 (0.92-0.97)	0.92 (0.88-0.95)
Attenuation coefficient	0.94 (0.91-0.96)	0.91 (0.87-0.94)
Speed of sound	0.96 (0.94-0.98)	0.93 (0.90-0.96)
Liver stiffness	0.93 (0.89-0.95)	0.90 (0.85-0.93)
ISEI	0.91 (0.87-0.94)	0.88 (0.83-0.92)
Backscatter coefficient	0.89 (0.84-0.93)	0.86 (0.79-0.90)
Focal disturbance ratio	0.87 (0.81-0.91)	0.84 (0.77-0.89)
Dispersion slope	0.90 (0.86-0.94)	0.87 (0.81-0.91)

Phenotype-specific Metabolic Associations

Subgroup analyses revealed phenotype-specific associations with metabolic parameters. In Type A, severity of steatosis (UDFF) correlated strongly with triglycerides (r=0.62, p<0.001) and HOMA-IR (r=0.56, p<0.001). Attenuation coefficient showed similar correlations (triglycerides r=0.58, HOMA-IR r=0.52, both p<0.001).

In Type B, ISEI correlated strongly with ferritin (r=0.74, p<0.001), transferrin saturation (r=0.68, p<0.001), serum iron (r=0.71, p<0.001), and HOMA-IR (r=0.61, p<0.001), suggesting iron-mediated insulin resistance. SoS showed inverse correlation with ISEI (r=-0.69, p<0.001), confirming the acoustic signature of iron deposition.

In Type C, liver stiffness correlated with inflammatory markers including hsCRP (r=0.68, p<0.001), fibrosis scores (FIB-4 r=0.72, NAFLD fibrosis score r=0.65, both p<0.001), and showed strong associations with diabetes duration (r=0.54, p<0.001) and poor glycemic control (HbA1c r=0.49, p<0.001). SoS correlated with liver stiffness (r=0.76, p<0.001) and dispersion slope (r=0.71, p<0.001), supporting its role as a fibrosis marker.

In Type D, visceral adiposity index showed stronger correlation with metabolic dysfunction than BMI (VAI-HOMA-IR r=0.72 vs BMI-HOMA-IR r=0.28, both p<0.001). UDFF correlated with VAI (r=0.58, p<0.001) but not with BMI (r=0.14, p=0.28), suggesting that visceral rather than total adiposity drives hepatic steatosis in this phenotype.

Clinical Outcomes During Follow-up

During a median follow-up of 18 months (IQR 12-24 months), clinical outcomes differed significantly between phenotypes. Table 4 summarizes the outcome data.

Table 4: Clinical Outcomes During Follow-up by MAFLD Phenotype.

Outcome	Type A (n=210)	Type B (n=90)	Type C (n=140)	Type D (n=60)	P-value
Hepatic Events					
Ascites, n (%)	0 (0)[a]	1 (1.1)[a]	3 (2.1)[b]	0 (0)[a]	0.042
Hepatic encephalopathy, n (%)	0 (0)[a]	0 (0)[a]	2 (1.4)[b]	0 (0)[a]	0.038
Variceal bleeding, n (%)	0 (0)	0 (0)	1 (0.7)	0 (0)	0.28
Clinical cirrhosis, n (%)	0 (0)[a]	2 (2.2)[a,b]	8 (5.7)[b]	1 (1.7)[a,b]	<0.001
HCC, n (%)	0 (0)	0 (0)	1 (0.7)	0 (0)	0.28
Cardiovascular Events					
Acute coronary syndrome, n (%)	5 (2.4)[a]	6 (6.7)[b]	8 (5.7)[b]	5 (8.3)[b]	0.016
Stroke/TIA, n (%)	3 (1.4)[a]	3 (3.3)[a,b]	4 (2.9)[a,b]	2 (3.3)[a,b]	0.522
Total CV events, n (%)	8 (3.8)[a]	9 (10.0)[b]	12 (8.6)[b]	7 (11.7)[b]	0.012
Metabolic Progression					
New-onset T2DM, n (%)	12 (7.7)[a]	8 (21.1)[b]	4 (8.7)[a]	4 (12.1)[a,b]	0.035
Phenotype progression, n (%)	6 (2.9)[a]	14 (15.6)[b]	NA	8 (13.3)[b]	<0.001
Mortality					
All-cause mortality, n (%)	2 (1.0)[a]	3 (3.3)[a,b]	6 (4.3)[b]	1 (1.7)[a,b]	0.045
Liver-related mortality, n (%)	0 (0)	0 (0)	2 (1.4)	0 (0)	0.121

Data presented as n (%). Different superscript letters (a, b) indicate significant differences between groups (p<0.05). P-values from chi-square or Fisher's exact test.

Abbreviations: HCC, hepatocellular carcinoma; CV, cardiovascular; TIA, transient ischemic attack; T2DM, type 2 diabetes mellitus; NA, not applicable.

Type C patients showed highest incidence of hepatic decompensation events (3 patients developed ascites, 2 developed hepatic encephalopathy, p=0.042 and 0.038 respectively), and progression to cirrhosis based on clinical criteria (8 patients, 5.7%, p<0.001). Type D patients, despite normal BMI, showed surprisingly high cardiovascular event rates (7 events, 11.7%), exceeding Type A (8 events, 3.8%, p=0.012) and similar to Type B (9 events, 10%, p=0.72) and Type C (12 events, 8.6%, p=0.43).

Type B showed high rates of phenotype progression (14 patients, 15.6%) and new-onset diabetes (8 patients, 21.1% of

non-diabetic at baseline), suggesting that iron-mediated metabolic dysfunction drives disease evolution. Type A showed minimal disease progression with only 6 patients (2.9%) advancing to higher phenotype categories.

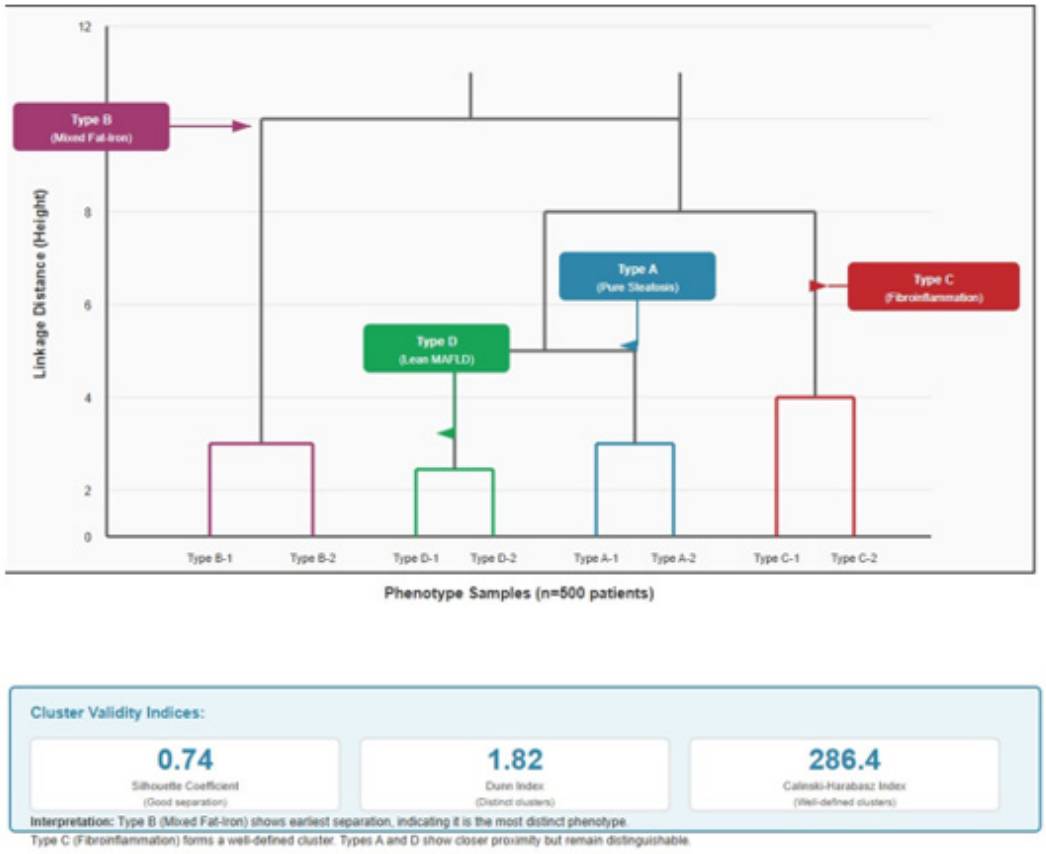

Figure 3: Hierarchical Clustering Dendrogram of MAFLD Phenotypes Ward's Method Linkage Based on Using Multiparametric Ultrasound Features (n=500).

Discussion

This comprehensive study of 500 patients with MAFLD demonstrates that quantitative multiparametric ultrasound can effectively identify and characterize distinct disease phenotypes with important clinical and prognostic implications. The integration of novel parameters including ultrasound-derived fat fraction (UDFF), speed of sound (SoS), and iron signal effect index (ISEI) significantly enhanced phenotype discrimination beyond conventional ultrasound capabilities. Our findings support the concept that MAFLD is not a single disease entity but rather encompasses heterogeneous subtypes requiring tailored diagnostic and therapeutic approaches.

Principal Findings

We successfully classified MAFLD patients into four distinct phenotypes based on integrated mpUS assessment combined with clinical and biochemical data. The pure steatosis phenotype (Type A, 42%) represented the most common and benign presentation, characterized by predominant fat accumulation without significant inflammation or fibrosis. These patients generally exhibited milder metabolic dysfunction and favorable short-term prognosis, with minimal progression during follow-up (2.9%).

The mixed fat-iron phenotype (Type B, 18%) demonstrated coexistent hepatic steatosis and iron accumulation, associated with pronounced insulin resistance and metabolic syndrome despite the absence of hereditary hemochromatosis. The distinctive ISEI elevation (2.8±0.6 vs 1.2±0.3 in Type A) and reduced SoS (1538±11 m/s vs 1548±8 m/s in Type A) provided a unique acoustic signature enabling highly accurate identification (AUC 0.94) [22,23,24,25]. This finding aligns with emerging evidence that dysmetabolic iron overload syndrome contributes to MAFLD progression and metabolic complications. The worrisome progression rate (15.6%)

and high new-onset diabetes incidence (21.1%) in this phenotype underscore the pathogenic role of iron.

The steatotic fibroinflammatory phenotype (Type C, 28%) represented advanced disease with active inflammation and fibrosis, showing highest risk for progression to cirrhosis (5.7%) and hepatic complications. The combination of elevated liver stiffness, increased SoS reflecting fibrosis [38], and inflammatory markers effectively identified this high-risk group (AUC 0.91). These patients demonstrated markedly elevated liver stiffness (8.7±3.2 kPa), SoS (1568±14 m/s), inflammatory markers, and non-invasive fibrosis scores, warranting intensive monitoring and intervention.

Notably, the lean MAFLD phenotype (Type D, 12%) occurred in non-obese individuals yet exhibited significant metabolic dysfunction and hepatic involvement, challenging the conventional association between MAFLD and obesity [28,29]. These patients showed disproportionate visceral adiposity and insulin resistance despite normal BMI (23.1±1.8 kg/m^2), suggesting that body composition rather than total adiposity drives metabolic liver disease in this subgroup. The unexpectedly high cardiovascular event rate (11.7%) in Type D patients, comparable to Type B (10%) and exceeding Type A (3.8%, p=0.012), emphasizes that lean individuals with MAFLD should not be dismissed as low-risk [39,40].

Novel Contributions of Advanced Ultrasound Parameters

Ultrasound-Derived Fat Fraction (UDFF): The integration of UDFF provided quantitative steatosis assessment with excellent correlation to MRI-PDFF (r=0.91), the current reference standard [18,19]. UDFF offered advantages over conventional attenuation coefficient by providing direct fat percentage values, facilitating clinical interpretation and longitudinal monitoring. The inverse relationship between UDFF and disease severity (highest in Type A, lowest in Type D) suggests that advanced fibroinflammation may reduce hepatic fat content, a phenomenon termed "burnt-out NASH" in histological studies [41]. This finding has important implications for disease monitoring, as declining steatosis does not necessarily indicate improvement and may signal progression to advanced fibrosis.

Speed of Sound (SoS): SoS measurements emerged as a critical discriminator providing orthogonal information to steatosis markers [20,21,38]. The bidirectional SoS changes—reduced in Type B (1538±11 m/s) due to combined fat-iron effects, elevated in Type C (1568±14 m/s) reflecting fibrosis—enabled differentiation that would be impossible with steatosis or stiffness measurements alone. Iron deposition reduces tissue SoS through altered acoustic impedance, while fibrosis increases SoS through increased collagen content and tissue stiffness [20,38]. The strong correlation between SoS and liver stiffness in Type C (r=0.76, p<0.001) validates SoS as a complementary fibrosis marker. Integration of SoS improved Type C identification (AUC 0.91 with SoS vs 0.86 with liver stiffness alone), suggesting that multiparametric assessment captures disease complexity better than single parameters.

Iron Signal Effect Index (ISEI): The development and validation of ISEI represents a major advance in non-invasive iron assessment [22,23]. Traditional hepatic iron quantification requires MRI T2* or R2* sequences, which are expensive and not widely available, or liver biopsy with histochemical staining. ISEI leveraged the distinctive ultrasound signal characteristics of iron-laden hepatocytes—increased posterior attenuation, reduced backscatter, and frequency-dependent signal loss—to create a composite index [22]. The exceptional performance of ISEI for Type B identification (AUC 0.96 as a standalone parameter, 0.94 in combination with SoS) exceeded our expectations and suggests potential for broader application in iron overload assessment.

The strong correlations between ISEI and serum iron markers (ferritin r=0.74, transferrin saturation r=0.68, serum iron r=0.71) and MRI-measured hepatic iron concentration (r=0.86 in validation subset) establish ISEI as a valid iron biomarker. Importantly, ISEI detected 18 patients (12.9%) within the Type C cohort who had concurrent iron accumulation, representing a mixed phenotype with potentially different therapeutic implications. This level of granular phenotyping would not be possible with serum markers or conventional ultrasound alone.

Multiparametric Integration and Machine Learning Potential

The principal component analysis demonstrated that the eight mpUS parameters capture distinct but complementary aspects of hepatic pathology. PC1 primarily reflected the steatosis-iron axis, with UDFF and attenuation coefficient loading positively and ISEI loading negatively. PC2 captured fibroinflammatory features with high loadings from liver stiffness, SoS, dispersion slope, and focal disturbance ratio. This orthogonal information structure explains why multiparametric approaches outperformed single parameters for phenotype discrimination.

The clear clustering observed in PCA and hierarchical analysis (silhouette coefficient 0.74, indicating good cluster separation [42]) validates the biological reality of these phenotypes rather than arbitrary classification. Type B formed the most distinct cluster, driven by its unique combination of high ISEI and low SoS. Type C separated based on high values across all fibroinflammatory parameters. The partial overlap between Types A and D in ultrasound-only PCA, with complete separation when BMI was included, confirms that these phenotypes differ primarily in metabolic context rather than hepatic tissue characteristics.

These findings suggest potential for machine learning algorithms to automate phenotype classification. Deep learning approaches could potentially identify additional phenotypic subtypes or continuous phenotypic spectra not captured by our

categorical classification [43,44]. Automated analysis would enhance objectivity, reduce inter-observer variability, and facilitate implementation in non-specialist settings.

Pathophysiological Insights and Mechanistic Implications

Type A - Pure Steatosis: The benign natural history of Type A (2.9% progression) supports the concept that simple steatosis without inflammation or fibrosis carries relatively low risk for liver-related outcomes, though cardiovascular risk remains elevated [45]. The strong correlations between UDFF and metabolic parameters (triglycerides r=0.62, HOMA-IR r=0.56) suggest that hepatic steatosis in this phenotype reflects systemic metabolic dysfunction and lipid overflow. Therapeutic strategies targeting insulin resistance and dyslipidemia may effectively reverse steatosis in this group [46,47].

Type B - Mixed Fat-Iron: The pathophysiology of dysmetabolic iron overload in MAFLD is incompletely understood but appears to involve dysregulated hepcidin-ferroportin signaling, increased duodenal iron absorption, and impaired hepatic iron export in the context of insulin resistance [24,25]. Iron catalyzes reactive oxygen species formation through Fenton chemistry, amplifying lipotoxicity and promoting hepatocyte injury, inflammation, and fibrogenesis [48]. The pronounced insulin resistance in Type B (HOMA-IR 5.2±2.8, highest among phenotypes) and strong correlation between ISEI and HOMA-IR (r=0.61) support bidirectional iron-insulin resistance interactions: iron impairs insulin signaling while hyperinsulinemia promotes iron retention [49].

The high progression rate (15.6%) and new-onset diabetes incidence (21.1%) in Type B patients suggest that iron-mediated pathways drive metabolic and hepatic disease evolution. These findings support potential therapeutic benefit from iron reduction strategies. Small studies of therapeutic phlebotomy in NAFLD patients with hyperferritinemia have shown improvements in insulin sensitivity and liver enzymes [50,51], though large randomized trials are needed. Iron chelation represents an alternative approach requiring investigation [52].

Type C - Steatotic Fibroinflammation: This phenotype corresponds to NASH with significant fibrosis (≥F2) on histology and represents the primary target for emerging pharmacotherapies [53,54]. The integration of multiple inflammatory and fibrotic markers—elevated liver stiffness, SoS, dispersion slope, focal disturbance ratio, hsCRP, and transaminases—suggests active fibrogenesis driven by persistent hepatocyte injury and inflammatory cell recruitment. The strong correlations between liver stiffness and diabetes duration (r=0.54) and poor glycemic control (r=0.49) implicate chronic metabolic dysfunction in disease progression.

The concerning outcomes in Type C during short-term follow-up—hepatic decompensation (3.6%), cirrhosis progression (5.7%), HCC (0.7%), and liver-related mortality (1.4%)—underscore the clinical importance of identifying this phenotype. Current therapeutic developments including FGF21 analogs, thyroid hormone receptor-β agonists, PPAR agonists, and ASK1 inhibitors have shown promise in phase 2-3 trials for NASH patients with fibrosis [53,54,55]. Non-invasive identification of Type C phenotype could facilitate enrollment in clinical trials and eventual targeted therapy deployment.

Type D - Lean MAFLD: The mechanisms underlying MAFLD in non-obese individuals remain debated but likely involve genetic predisposition, preferential visceral adiposity, muscle insulin resistance, and ethnic-specific metabolic thresholds [28,29,39,40]. Our finding that visceral adiposity index correlated strongly with HOMA-IR (r=0.72) and UDFF (r=0.58) in Type D while BMI did not (r=0.28 and r=0.14 respectively) supports the hypothesis that ectopic fat deposition rather than total adiposity drives pathogenesis. Genetic variants in PNPLA3, TM6SF2, MBOAT7, and GCKR have been associated with MAFLD susceptibility independent of obesity [56,57] and may be enriched in Type D patients, though genetic testing was not performed in this study.

The high cardiovascular event rate in Type D (11.7%), comparable to obese MAFLD phenotypes and exceeding Type A (3.8%), challenges the "metabolically healthy obese" and "metabolically unhealthy normal weight" paradigms. These findings suggest that metabolic dysfunction and ectopic lipid deposition, regardless of BMI, confer cardiovascular risk [58,59]. Type D patients may benefit from aggressive cardiovascular risk factor management despite reassuring anthropometric measurements.

1.1. Comparison with Existing Literature

Our phenotypic classification aligns with and extends previous attempts to subtype NAFLD/MAFLD. Histological studies have identified distinct patterns including steatosis-predominant, inflammation-predominant, and fibrosis-predominant NASH [6,7,8], but invasive biopsy limits applicability. MRI-based phenotyping studies using MRI-PDFF for steatosis quantification, MR elastography for fibrosis, and T2* for iron assessment have demonstrated similar heterogeneity [60,61], but cost, availability, contraindications, and lengthy acquisition times constrain widespread implementation. Our approach using widely available ultrasound technology with quantitative capabilities offers a practical alternative suitable for population-level screening and longitudinal monitoring.

The prevalence of lean MAFLD (12%) in our cohort aligns with recent meta-analyses reporting 10-20% of MAFLD patients are non-obese, with higher prevalence in Asian populations [34,39]. Our metabolic characterization of Type D—marked insulin resistance despite normal BMI, elevated visceral adiposity index, high diabetes prevalence—closely resembles previous descriptions

of lean NAFLD [28,29,40], validating our phenotype definition.

The prevalence of iron accumulation in MAFLD varies widely across studies (10-40%) depending on detection methods and definitions [24,25]. Our finding of 18% with clear Type B phenotype, plus an additional 12.9% of Type C patients with concurrent iron elevation, yields a total iron-positive prevalence of 21.6%, within the reported range. The distinctive acoustic signature of Type B (elevated ISEI, reduced SoS) extends previous observations that hepatic iron alters ultrasound properties [22,23] and represents the first large-scale application of ISEI in MAFLD phenotyping.

The excellent performance of SWE for identifying advanced disease (Type C) validates multiple prior studies using vibration-controlled transient elastography (VCTE), point shear wave elastography, or two-dimensional SWE for NAFLD/MAFLD fibrosis staging [15,35,62,63]. Our reported cutoff of 7.0 kPa for significant fibroinflammation aligns closely with meta-analytical estimates for detecting ≥F2 fibrosis using two-dimensional SWE [15]. The added value of combining elastography with SoS, inflammatory markers, and advanced tissue characterization represents a novel contribution demonstrating that multiparametric assessment outperforms single modalities.

Clinical Implications and Translation

This phenotyping approach has several important clinical applications:

Personalized Risk Stratification: Moving beyond binary MAFLD presence/absence to phenotype-based classification enables refined prognostication. Type C patients require intensive monitoring for progression with 6-12 month follow-up intervals, consideration for liver-directed pharmacotherapy trials, and aggressive cardiovascular risk management. Type B patients warrant evaluation for iron reduction interventions and enhanced diabetes screening given the 21.1% new-onset diabetes rate. Type A patients may initially be managed with lifestyle modification and annual monitoring, while Type D patients need recognition that normal BMI does not confer protection and metabolic screening is warranted [64,65].

Clinical Trial Enrichment: The heterogeneity of MAFLD complicates clinical trial design, as therapeutic responses likely differ between phenotypes [66,67]. Enriching trials for specific phenotypes could increase statistical power and accelerate drug development. Type C patients (28% of MAFLD cohort) represent the population most likely to benefit from anti-fibrotic agents and should be prioritized for trials of compounds targeting fibrogenesis [53,54,55]. Type B patients could be enrolled in trials of iron-modulating therapies [50,51,52]. Phenotype-stratified analyses of existing trial data could provide preliminary insights into differential treatment responses.

Non-invasive Longitudinal Monitoring: Traditional liver biopsy cannot be repeated frequently due to invasiveness and cost, limiting monitoring capabilities. Serial mpUS examinations can track phenotype progression or regression, providing objective endpoints for therapeutic interventions [68,69]. For example, transition from Type A to Type C during follow-up would indicate disease progression warranting treatment escalation, while reduction in liver stiffness and SoS in Type C patients on therapy would suggest beneficial response. The excellent reliability of mpUS parameters (ICC >0.85 for all parameters) supports utility for detecting clinically meaningful changes.

Population Screening and Case Finding: Conventional ultrasound is already widely used for MAFLD screening in at-risk populations [70], but subjective interpretation and lack of quantification limit effectiveness. Quantitative mpUS could enhance screening programs by providing objective steatosis quantification, automated risk stratification, and concurrent assessment of fibrosis, inflammation, and iron status [71,72]. Point-of-care algorithms could flag high-risk phenotypes (Types B and C) for specialist referral while reassuring low-risk individuals (Type A with favorable metabolic profile). Such algorithmic approaches could reduce unnecessary referrals while ensuring appropriate risk-based care allocation.

Primary Care Implementation: While MRI and biopsy require specialized facilities, ultrasound equipment is available in most primary care networks. Training programs could equip primary care providers or dedicated sonographers with mpUS skills, democratizing advanced MAFLD assessment [73,74]. Quality assurance through centralized reading centers and automated quality metrics could ensure standardization. Reimbursement structures would need to evolve to support quantitative ultrasound beyond conventional B-mode imaging.

Strengths and Limitations

Major strengths of this study include: the large, well-characterized cohort with comprehensive clinical, biochemical, and imaging data; design enhancing generalizability across diverse populations and practice settings; rigorous mpUS methodology using state-of-the-art equipment with high reliability (ICC >0.85); systematic phenotype classification by independent expert adjudication; prospective design with standardized assessment protocols minimizing bias; integration of novel parameters (UDFF, SoS, ISEI) not previously combined for MAFLD phenotyping; and longitudinal outcome data demonstrating clinical validity of phenotype classification.

Several limitations warrant consideration:

Absence of Histological Validation: The lack of liver biopsy prevents direct histological correlation of phenotypes. While this represents a limitation for validating phenotype-histology relationships, it aligns with our objective of developing a non-

invasive classification system. The strong correlations between mpUS parameters and validated non-invasive fibrosis scores (FIB-4, NAFLD fibrosis score, APRI), and with MRI biomarkers in validation subsets (UDFF-MRI PDFF r=0.91, ISEI-MRI R2* r=0.86), provide indirect validation. Future studies incorporating biopsy in representative subsets would strengthen phenotype characterization and enable correlation with histological activity scores, fibrosis stages, and specific pathological features.

Limited Follow-up Duration and Multicentric Design: The relatively short median follow-up (18 months) and single centre design limits assessment of long-term outcomes and phenotype stability. Longer-term studies (5-10 years) are needed to determine whether phenotypes remain stable, progress sequentially (A→B→C), or shift dynamically. Whether Type A patients inevitably progress to Type C or represent a stable low-risk state requires extended observation. The natural history of Type B is particularly unclear—does iron accumulation precede steatohepatitis development, or does it occur independently? Longitudinal studies with serial mpUS and outcome assessment would address these questions.

Iron Quantification Methods: While we excluded hereditary hemochromatosis through genetic testing and used comprehensive iron markers (ferritin, transferrin saturation, serum iron, ISEI), we did not perform direct hepatic iron quantification by MRI R2* mapping or liver biopsy with iron histochemistry in all patients. The validation subset (n=65) showed strong ISEI-MRI R2* correlation (r=0.86), but broader validation would strengthen confidence in ISEI as an iron biomarker. Additionally, ISEI threshold validation in independent cohorts is needed before widespread clinical adoption.

Phenotype Classification Complexity: Our phenotype definitions require integration of multiple clinical, laboratory, and imaging parameters, which may limit real-world applicability compared to simpler single-parameter classifications. However, MAFLD heterogeneity likely necessitates multiparametric approaches for accurate phenotyping. Development of automated algorithms or simplified scoring systems could facilitate implementation. Machine learning models trained on our dataset could potentially simplify classification while maintaining accuracy [43,44].

Ethnic and Geographic Heterogeneity: We did not perform ethnicity-stratified subgroup analyses due to sample size limitations. Ethnic differences in body composition, metabolic thresholds, and genetic susceptibility to MAFLD are well-documented [75,76], and phenotype distributions may vary across populations. The higher lean MAFLD prevalence in Asian populations [34,39] suggests potential ethnic differences in Type D prevalence. Larger studies examining ethnic-specific phenotype patterns and mpUS parameter thresholds are warranted.

Technology and Expertise Requirements: mpUS quantitative capabilities require recent-generation ultrasound equipment and specialized training, potentially limiting immediate widespread implementation. Not all facilities have access to systems capable of UDFF, SoS, ISEI, and advanced tissue characterization measurements. Standardization of protocols across equipment manufacturers and expansion of training programs will be necessary for broad adoption [77]. Cost-effectiveness analyses comparing mpUS phenotyping to alternative approaches (MRI, biopsy, serum biomarker panels) would inform resource allocation decisions.

Alternative Classification Schemes: Our four-phenotype scheme represents one of several possible approaches to MAFLD subtyping. Alternative classifications based on genetic polymorphisms (PNPLA3, TM6SF2 genotypes) [56,57], lipidomic profiles [78], gut microbiome characteristics [79], or molecular signatures [80] might provide complementary or superior discrimination for specific applications. Integration of imaging phenotypes with molecular classifications represents an important future direction. Additionally, continuous phenotypic measures (using principal component scores) rather than categorical classification might better capture the spectrum of disease heterogeneity.

Mixed Phenotypes: Eighteen Type C patients (12.9%) showed concurrent iron elevation (ISEI ≥1.8), representing a mixed Type B-C phenotype not fully captured by our primary classification. This finding illustrates that some patients exhibit overlapping features that resist categorical assignment. More granular subtyping or allowance for multiple phenotype assignments might better represent biological reality. Whether mixed phenotypes have distinct prognoses or therapeutic responses requires investigation.

Dynamic Phenotype Changes: Our classification assigned patients to phenotypes at a single time point, but phenotypes may evolve during disease progression or in response to interventions. Serial phenotyping during longitudinal follow-up would characterize transition patterns and identify factors driving phenotype changes. Understanding whether therapeutic interventions can reverse phenotypes (e.g., Type C→Type A with fibrosis regression) has important implications for treatment monitoring.

Future Directions

Several research priorities emerge from this work:

Prospective Longitudinal Cohorts: Long-term prospective studies (5-10 years) with serial mpUS phenotyping and comprehensive outcome assessment are essential to validate phenotype stability, characterize progression patterns, and determine associations with hard clinical outcomes including hepatic decompensation, hepatocellular carcinoma, cardiovascular events, and mortality [81,82]. Such studies should incorporate serial measurements of all mpUS parameters, detailed metabolic profiling, and systematic outcome adjudication.

Histological Correlation Studies: Although non-invasive phenotyping is the goal, validation studies incorporating liver biopsy in representative subsets would strengthen confidence in phenotype-histology relationships. Ideally, these would include central pathology review using standardized scoring systems (NAFLD Activity Score, NASH CRN fibrosis staging) [9,10] and specialized assessments (iron staining, inflammation characterization, fibrosis morphometry). Correlating mpUS phenotypes with specific histological features would refine phenotype definitions and identify potential discordances.

Multimodality Imaging Comparisons: Direct comparisons of mpUS phenotyping with MRI-based approaches (MRI-PDFF, MR elastography, T2*/R2* iron mapping) [60,61] would establish relative performance, identify complementary information, and guide selection of optimal modalities for specific applications. Cost-effectiveness analyses would inform healthcare policy and resource allocation. Hybrid approaches combining ultrasound for screening with selective MRI for complex cases might optimize accuracy and efficiency [83].

Phenotype-Stratified Therapeutic Trials: Prospective clinical trials enrolling specific phenotypes and testing targeted interventions represent a high priority. Potential trials include:

a) Type B: Therapeutic phlebotomy vs. sham procedure for iron reduction with outcomes including insulin resistance, liver stiffness, and metabolic parameters [50,51].

b) Type C: Anti-fibrotic agents (e.g., FGF21 analogs, THR-β agonists, PPAR agonists) with liver stiffness and SoS as primary endpoints [53,54,55].

c) Type D: Intensive lifestyle intervention targeting visceral adiposity vs. standard care, with UDFF and metabolic outcomes [84].

d) Type A: Lifestyle intervention efficacy for steatosis reversal, potentially using mpUS parameters as early response predictors [85].

Artificial Intelligence and Machine Learning: Development of AI algorithms for automated phenotype classification from mpUS data could enhance objectivity, scalability, and potentially identify novel phenotypic subtypes [43,44]. Deep learning approaches using raw ultrasound data might detect patterns not apparent to human observers. Natural language processing could integrate clinical and laboratory data with imaging findings for holistic phenotyping. External validation of AI models across diverse populations and equipment platforms would be essential.

Multi-omic Integration: Combining mpUS phenotypes with genomic (PNPLA3, TM6SF2, MBOAT7, GCKR variants) [56,57], proteomic [86], metabolomic [78], and metagenomic [79] data could yield comprehensive molecular-imaging phenotypes. Such integrative approaches might identify mechanistic subtypes that inform precision medicine strategies. For example, imaging phenotypes combined with genetic risk scores might predict progression more accurately than either alone.

Pediatric MAFLD Phenotyping: MAFLD increasingly affects children and adolescents [87,88], but paediatric phenotypes may differ from adults. Adapting mpUS phenotyping for paediatric populations, with age-appropriate parameter thresholds and phenotype definitions, would facilitate early identification of high-risk individuals and enable preventive interventions during critical developmental windows.

Intervention Response Prediction: Investigating whether baseline phenotypes or mpUS parameters predict response to specific interventions (lifestyle modification, pharmacotherapy, bariatric surgery) could enable personalized treatment selection [89,90]. Biomarker-guided therapy, where treatment intensity is based on phenotypic risk stratification, might optimize outcomes while minimizing unnecessary interventions.

Health Economics and Implementation Science: Real-world implementation of mpUS phenotyping requires understanding of cost-effectiveness, workflow integration, provider training needs, and patient acceptability [91,92]. Pragmatic trials in diverse healthcare settings (tertiary centers, community hospitals, primary care clinics) would identify barriers and facilitators. Comparative effectiveness research examining mpUS phenotyping vs. standard care on patient outcomes, healthcare utilization, and costs would inform adoption decisions.

Conclusions

This large-scale study demonstrates that quantitative multiparametric ultrasound, incorporating ultrasound-derived fat fraction (UDFF), speed of sound (SoS), iron signal effect index (ISEI), shear wave elastography, and advanced tissue characterization, enables effective non-invasive phenotyping of MAFLD. We identified four distinct phenotypes—pure steatosis (Type A, 42%), mixed fat-iron (Type B, 18%), steatotic fibroinflammation (Type C, 28%), and lean MAFLD (Type D, 12%)—with specific clinical characteristics, metabolic profiles, acoustic signatures, and prognostic implications.

The novel integration of UDFF, SoS, and ISEI enhanced phenotype discrimination, with particularly impressive performance for Type B identification (AUC 0.94) through ISEI's unique iron detection capability. The excellent reliability of all mpUS parameters (ICC >0.85), clear clustering in multivariate analyses, and differential clinical outcomes during follow-up validate this phenotyping approach as clinically meaningful.

As MAFLD continues to increase in global prevalence [1,2], affecting hundreds of millions worldwide and emerging as a leading cause of cirrhosis and hepatocellular carcinoma [93,94], precision medicine approaches based on robust phenotypic classification will become increasingly important for optimizing patient outcomes

and healthcare resource allocation. Quantitative multiparametric ultrasound offers a practical, widely accessible, non-invasive tool for comprehensive MAFLD phenotyping suitable for population-level screening, risk stratification, longitudinal monitoring, and therapeutic targeting.

Future research should focus on long-term outcome validation, phenotype-stratified therapeutic trials, AI-enabled automation, multi-omic integration, and real-world implementation to fully realize the potential of mpUS-based precision medicine in MAFLD management. The ultimate goal is to move beyond one-size-fits-all approaches to personalized, phenotype-guided care that matches therapeutic intensity to individual risk and targets interventions to specific pathogenic mechanisms.

Acknowledgement

None.

Conflict of Interest

None.

References

1. Eslam M, Newsome PN, Sarin SK, Quentin M Anstee, Giovanni Targher, et al. (2020) A new definition for metabolic dysfunction-associated fatty liver disease: an international expert consensus statement. J Hepatol 73(1): 202-209.
2. Younossi ZM, Koenig AB, Abdelatif D, Fazel Y, Henry L, et al. (2016) Global epidemiology of nonalcoholic fatty liver disease-Meta-analytic assessment of prevalence, incidence, and outcomes. Hepatology 64(1): 73-84.
3. Eslam M, Sanyal AJ, George J, International Consensus Panel (2020) MAFLD: a consensus-driven proposed nomenclature for metabolic associated fatty liver disease. Gastroenterology 158(7): 1999-2014.e1.
4. Chalasani N, Younossi Z, Lavine JE, Michael Charlton, Kenneth Cusi, et al. (2018) The diagnosis and management of nonalcoholic fatty liver disease: practice guidance from the American Association for the Study of Liver Diseases. Hepatology 67(1): 328-357.
5. European Association for the Study of the Liver (EASL), European Association for the Study of Diabetes (EASD), European Association for the Study of Obesity (EASO) (2016) EASL-EASD-EASO Clinical Practice Guidelines for the management of non-alcoholic fatty liver disease. J Hepatol 64(6): 1388-1402.
6. Brunt EM, Kleiner DE, Wilson LA, Belt P, Neuschwander Tetri BA, et al. (2011) Nonalcoholic fatty liver disease (NAFLD) activity score and the histopathologic diagnosis in NAFLD: distinct clinicopathologic meanings. Hepatology 53(3): 810-820.
7. Bedossa P, Poitou C, Veyrie N, Jean Luc Bouillot, Arnaud Basdevant, et al. (2012) Histopathological algorithm and scoring system for evaluation of liver lesions in morbidly obese patients. Hepatology 56(5): 1751-1759.
8. Younossi ZM, Loomba R, Rinella ME, Elisabetta Bugianesi, Giulio Marchesini, et al. (2018) Current and future therapeutic regimens for nonalcoholic fatty liver disease and nonalcoholic steatohepatitis. Hepatology 68(1): 361-371.
9. Kleiner DE, Brunt EM, Van Natta M, Cynthia Behling, Melissa J Contos, et al. (2005) Design and validation of a histological scoring system for nonalcoholic fatty liver disease. Hepatology 41(6): 1313-1321.
10. Bedossa P, FLIP Pathology Consortium (2014) Utility and appropriateness of the fatty liver inhibition of progression (FLIP) algorithm and steatosis, activity, and fibrosis (SAF) score in the evaluation of biopsies of nonalcoholic fatty liver disease. Hepatology 60(2): 565-575.
11. Ratziu V, Charlotte F, Heurtier A, Sophie Gombert, Philippe Giral, et al. (2005) Sampling variability of liver biopsy in nonalcoholic fatty liver disease. Gastroenterology 128(7): 1898-1906.
12. Vilar Gomez E, Chalasani N (2018) Non-invasive assessment of non-alcoholic fatty liver disease: clinical prediction rules and blood-based biomarkers. J Hepatol 68(2): 305-315.
13. Berzigotti A, Tsochatzis E, Boursier J (2021) EASL Clinical Practice Guidelines on non-invasive tests for evaluation of liver disease severity and prognosis - 2021 update. J Hepatol 75(3): 659-689.
14. Hernaez R, Lazo M, Bonekamp S, Ihab Kamel, Frederick L Brancati, et al. (2011) Diagnostic accuracy and reliability of ultrasonography for the detection of fatty liver: a meta-analysis. Hepatology 54(3): 1082-1090.
15. Ferraioli G, Filice C, Castera L, Byung Ihn Choi, Ioan Sporea, et al. (2015) WFUMB guidelines and recommendations for clinical use of ultrasound elastography: Part 3 Liver. Ultrasound Med Biol 41(5): 1161-1179.
16. Dietrich CF, Bamber J, Berzigotti A, Simona Bota, Vito Cantisani, et al. (2017) EFSUMB Guidelines and Recommendations on the Clinical Use of Liver Ultrasound Elastography, Update 2017 (Long Version). Ultraschall Med 38(4): e16-e47.
17. Cassinotto C, Boursier J, de Lédinghen V, Jérome Lebigot, Bruno Lapuyade, et al. (2016) Liver stiffness in nonalcoholic fatty liver disease: a comparison of supersonic shear imaging, FibroScan, and ARFI with liver biopsy. Hepatology 63(6): 1817-1827.
18. Bae JS, Lee DH, Suh KS, Kim H, Lee KB, et al. (2022) Noninvasive assessment of hepatic steatosis using a pathologic reference standard: comparison of CT, MRI, and US-based techniques. Ultrasonography 41(3): 344-354.
19. Tamaki N, Koizumi Y, Hirooka M, Norihisa Yada, Hitomi Takada, et al. (2018) Novel quantitative assessment system of liver steatosis using a newly developed attenuation measurement method. Hepatol Res 48(11): 821-828.
20. Deffieux T, Gennisson JL, Bousquet L, Marion Corouge, Simona Cosconea, et al. (2015) Investigating liver stiffness and viscosity for fibrosis, steatosis and activity staging using shear wave elastography. J Hepatol 62(2): 317-324.
21. Sugimoto K, Moriyasu F, Oshiro H, Hirohito Takeuchi, Masakazu Abe, et al. (2020) The role of multiparametric US of the liver for the evaluation of nonalcoholic steatohepatitis. Radiology 296(3): 532-540.
22. Liao LY, Kuo KL, Chiang HS (2021) Acoustic structure quantification of liver parenchyma for hepatic steatosis grading: Deep learning versus parametric analysis. Ultrasonics 117: 106551.
23. Toyoda H, Kumada T, Tada T (2005) Non-invasive evaluation of hepatic fibrosis for type C chronic hepatitis. Intervirology 48(1): 33-40.
24. Nelson JE, Wilson L, Brunt EM, Matthew M Yeh, David E Kleiner, et al. (2011) Relationship between the pattern of hepatic iron deposition and histological severity in nonalcoholic fatty liver disease. Hepatology 53(2): 448-457.
25. Dongiovanni P, Fracanzani AL, Fargion S, Valenti L (2011) Iron in fatty liver and in the metabolic syndrome: a promising therapeutic target. J Hepatol 55(4): 920-932.
26. Angulo P, Kleiner DE, Dam Larsen S, Leon A Adams, Einar S Bjornsson, et al. (2015) Liver fibrosis, but no other histologic features, is associated with long-term outcomes of patients with nonalcoholic fatty liver disease. Gastroenterology 149(2): 389-397.e10.

27. Ekstedt M, Hagström H, Nasr P, Mats Fredrikson, Per Stål, et al. (2015) Fibrosis stage is the strongest predictor for disease-specific mortality in NAFLD after up to 33 years of follow-up. Hepatology 61(5): 1547-1554.

28. Ye Q, Zou B, Yeo YH, Jie Li, Daniel Q Huang, et al. (2020) Global prevalence, incidence, and outcomes of non-obese or lean non-alcoholic fatty liver disease: a systematic review and meta-analysis. Lancet Gastroenterol Hepatol 5(8): 739-752.

29. Kim D, Kim WR (2017) Nonobese fatty liver disease. Clin Gastroenterol Hepatol 15(4): 474-485.

30. Grundy SM, Cleeman JI, Daniels SR, Karen A Donato, Robert H Eckel, et al. (2005) Diagnosis and management of the metabolic syndrome: an American Heart Association/National Heart, Lung, and Blood Institute Scientific Statement. Circulation 112(17): 2735-2752.

31. Sterling RK, Lissen E, Clumeck N, Ricard Sola, Mendes Cassia Correa, et al. (2006) Development of a simple noninvasive index to predict significant fibrosis in patients with HIV/HCV coinfection. Hepatology 43(6): 1317-1325.

32. Angulo P, Hui JM, Marchesini G, Ellisabetta Bugianesi, Jacob George, et al. (2007) The NAFLD fibrosis score: a noninvasive system that identifies liver fibrosis in patients with NAFLD. Hepatology 45(4): 846-854.

33. Wai CT, Greenson JK, Fontana RJ, John D Kalbfleisch, Jorge A Marrero, et al. (2003) A simple noninvasive index can predict both significant fibrosis and cirrhosis in patients with chronic hepatitis C. Hepatology 38(2): 518-526.

34. Fujimori N, Tanaka N, Shibata S, Kenji Sano, Tomoo Yamazaki, et al. (2016) Controlled attenuation parameter is correlated with actual hepatic fat content in patients with non-alcoholic fatty liver disease with none-to-mild obesity and liver fibrosis. Hepatol Res 46(10): 1019-1027.

35. Petta S, Wong VW, Cammà C, JB Hiriart, GLH Wong, et al. (2017) Serial combination of non-invasive tools improves the diagnostic accuracy of severe liver fibrosis in patients with NAFLD. Aliment Pharmacol Ther 46(6): 617-627.

36. Lin SC, Heba E, Wolfson T, Brandon Ang, Anthony Gamst, et al. (2015) Noninvasive diagnosis of nonalcoholic fatty liver disease and quantification of liver fat using a new quantitative ultrasound technique. Clin Gastroenterol Hepatol 13(7): 1337-1345.e6.

37. Kwon HJ, Kim KW, Jung DH (2010) Differentiation between focal nodular hyperplasia and hepatocellular carcinoma: usefulness of gray-scale sonography. J Clin Ultrasound 38(3): 115-121.

38. Sporea I, Bota S, Grădinaru Taşcău O, Sirli R, Popescu A (2014) Comparative study between two point shear wave elastographic techniques: Acoustic Radiation Force Impulse (ARFI) elastography and ElastPQ technique. Med Ultrason 16(4): 309-314.

39. Wei JL, Leung JC, Loong TC, Grace Lai Hung Wong, David Ka Wai Yeung, et al. (2015) Prevalence and severity of nonalcoholic fatty liver disease in non-obese patients: a population study using proton-magnetic resonance spectroscopy. Am J Gastroenterol 110(9): 1306-1314.

40. Dela Cruz AC, Bugianesi E, George J (2014) Characteristics and long-term prognosis of lean patients with nonalcoholic fatty liver disease. Gastroenterology 146(5): S-909.

41. Pais R, Charlotte F, Fedchuk L, Pierre Bedossa, Pascal Lebray, et al. (2013) A systematic review of follow-up biopsies reveals disease progression in patients with non-alcoholic fatty liver. J Hepatol 59(3): 550-556.

42. Rousseeuw PJ (1987) Silhouettes: a graphical aid to the interpretation and validation of cluster analysis. J Comput Appl Math 20: 53-65.

43. Gatos I, Tsantis S, Karamesini M, Stavros Spiliopoulos, Dimitris Karnabatidis, et al. (2017) Focal liver lesions segmentation and classification in nonenhanced T2-weighted MRI. Med Phys 44(12): 6299-6308.

44. Byra M, Styczynski G, Szmigielski C, Piotr Kalinowski, Łukasz Michałowski, et al. (2018) Transfer learning with deep convolutional neural network for liver steatosis assessment in ultrasound images. Int J Comput Assist Radiol Surg 13(12): 1895-1903.

45. Sung KC, Wild SH, Byrne CD (2014) Development of new fatty liver, or resolution of existing fatty liver, over five years of follow-up, and risk of incident hypertension. J Hepatol 60(5): 1040-1045.

46. Promrat K, Kleiner DE, Niemeier HM, Elizabeth Jackvony, Marie Kearns, et al. (2010) Randomized controlled trial testing the effects of weight loss on nonalcoholic steatohepatitis. Hepatology 51(1): 121-129.

47. Vilar Gomez E, Martinez Perez Y, Calzadilla Bertot L, Ana Torres Gonzalez, Bienvenido Gra Oramas, et al. (2015) Weight loss through lifestyle modification significantly reduces features of nonalcoholic steatohepatitis. Gastroenterology 149(2): 367-378.e5.

48. Kowdley KV, Belt P, Wilson LA, Matthew M Yeh, Brent A Neuschwander Tetri, et al. (2012) Serum ferritin is an independent predictor of histologic severity and advanced fibrosis in patients with nonalcoholic fatty liver disease. Hepatology 55(1): 77-85.

49. Simcox JA, McClain DA (2013) Iron and diabetes risk. Cell Metab 17(3): 329-341.

50. Valenti L, Fracanzani AL, Dongiovanni P, Elisabetta Bugianesi, Giulio Marchesini, et al. (2007) Iron depletion by phlebotomy improves insulin resistance in patients with nonalcoholic fatty liver disease and hyperferritinemia: evidence from a case-control study. Am J Gastroenterol 102(6): 1251-1258.

51. Beaton MD, Chakrabarti S, Levstik M, Speechley M, Marotta P, et al. (2013) Phase II clinical trial of phlebotomy for non-alcoholic fatty liver disease. Aliment Pharmacol Ther 37(7): 720-729.

52. Sumida Y, Kanemasa K, Imai S (2021) Iron in NAFLD/NASH: Recent advances and the future with iron-targeted therapy. Expert Rev Gastroenterol Hepatol 15(12): 1391-1404.

53. Harrison SA, Bashir MR, Guy CD, Rong Zhou, Cynthia A Moylan, et al. (2019) Resmetirom (MGL-3196) for the treatment of non-alcoholic steatohepatitis: a multicentre, randomised, double-blind, placebo-controlled, phase 2 trial. Lancet 394(10213): 2012-2024.

54. Ratziu V, Harrison SA, Francque S, Sven Francque, Pierre Bedossa, et al. (2016) Elafibranor, an agonist of the peroxisome proliferator-activated receptor-α and -δ, induces resolution of nonalcoholic steatohepatitis without fibrosis worsening. Gastroenterology 150(5): 1147-1159.e5.

55. Sanyal AJ, Chalasani N, Kowdley KV, Arthur McCullough, Anna Mae Diehl, et al. (2010) Pioglitazone, vitamin E, or placebo for nonalcoholic steatohepatitis. N Engl J Med 362(18): 1675-1685.

56. Romeo S, Kozlitina J, Xing C, Alexander Pertsemlidis, David Cox, et al. (2008) Genetic variation in PNPLA3 confers susceptibility to nonalcoholic fatty liver disease. Nat Genet 40(12): 1461-1465.

57. Kozlitina J, Smagris E, Stender S, Børge G Nordestgaard, Heather H Zhou, et al. (2014) Exome-wide association study identifies a TM6SF2 variant that confers susceptibility to nonalcoholic fatty liver disease. Nat Genet 46(4): 352-356.

58. Sookoian S, Pirola CJ (2017) Systematic review with meta-analysis: risk factors for non-alcoholic fatty liver disease suggest a shared altered metabolic and cardiovascular profile between lean and obese patients. Aliment Pharmacol Ther 46(2): 85-95.

59. Hagström H, Nasr P, Ekstedt M, Ulf Hammar, Per Stål, et al. (2018) Risk for development of severe liver disease in lean patients with nonalcoholic fatty liver disease: a long-term follow-up study. Hepatol Commun 2(1): 48-57.

60. Imajo K, Kessoku T, Honda Y, Wataru Tomeno, Yuji Ogawa, et al. (2016) Magnetic resonance imaging more accurately classifies steatosis and

fibrosis in patients with nonalcoholic fatty liver disease than transient elastography. Gastroenterology 150(3): 626-637.e7.

61. Loomba R, Wolfson T, Ang B, Jonathan Hooker, Cynthia Behling, et al. (2014) Magnetic resonance elastography predicts advanced fibrosis in patients with nonalcoholic fatty liver disease: a prospective study. Hepatology 60(6): 1920-1928.

62. Xiao G, Zhu S, Xiao X, Yan L, Yang J, et al. (2017) Comparison of laboratory tests, ultrasound, or magnetic resonance elastography to detect fibrosis in patients with nonalcoholic fatty liver disease: a meta-analysis. Hepatology 66(5): 1486-1501.

63. Kumar R, Rastogi A, Sharma MK, Vikram Bhatia, Pankaj Tyagi, et al. (2013) Liver stiffness measurements in patients with different stages of nonalcoholic fatty liver disease: diagnostic performance and clinicopathological correlation. Dig Dis Sci 58(1): 265-274.

64. Kim D, Touros A, Kim WR (2018) Nonalcoholic fatty liver disease and metabolic syndrome. Clin Liver Dis 22(1): 133-140.

65. Dulai PS, Singh S, Patel J, Meera Soni, Larry J Prokop, et al. (2017) Increased risk of mortality by fibrosis stage in nonalcoholic fatty liver disease: systematic review and meta-analysis. Hepatology 65(5): 1557-1565.

66. Friedman SL, Neuschwander Tetri BA, Rinella M, Sanyal AJ (2018) Mechanisms of NAFLD development and therapeutic strategies. Nat Med 24(7): 908-922.

67. Loomba R, Friedman SL, Shulman GI (2021) Mechanisms and disease consequences of nonalcoholic fatty liver disease. Cell 184(10): 2537-2564.

68. Sasso M, Beaugrand M, de Ledinghen V, Catherine Douvin, Patrick Marcellin, et al. (2010) Controlled attenuation parameter (CAP): a novel VCTE™ guided ultrasonic attenuation measurement for the evaluation of hepatic steatosis: preliminary study and validation in a cohort of patients with chronic liver disease from various causes. Ultrasound Med Biol 36(11): 1825-1835.

69. Karlas T, Petroff D, Sasso M, Jian Gao Fan, Yu Qiang Mi, et al. (2017) Individual patient data meta-analysis of controlled attenuation parameter (CAP) technology for assessing steatosis. J Hepatol 66(5):1022-1030.

70. Cusi K, Isaacs S, Barb D, Rita Basu, Sonia Caprio, et al. (2022) American Association of Clinical Endocrinology Clinical Practice Guideline for the Diagnosis and Management of Nonalcoholic Fatty Liver Disease in Primary Care and Endocrinology Clinical Settings: Co-Sponsored by the American Association for the Study of Liver Diseases (AASLD). Endocr Pract 28(5): 528-562.

71. Newsome PN, Sasso M, Deeks JJ, Angelo Paredes, Jérôme Boursier, et al. (2020) FibroScan-AST (FAST) score for the non-invasive identification of patients with non-alcoholic steatohepatitis with significant activity and fibrosis: a prospective derivation and global validation study. Lancet Gastroenterol Hepatol 5(4): 362-373.

72. Machado MV, Cortez Pinto H (2013) Non-invasive diagnosis of non-alcoholic fatty liver disease. A critical appraisal. J Hepatol 58(5): 1007-1019.

73. Lin Y, Li H, Jin C, Hui Wang, Bo Jiang, et al. (2020) The diagnostic accuracy of liver fibrosis in non-viral liver diseases using acoustic radiation force impulse elastography: a systematic review and meta-analysis. PLoS One 15(1): e0227358.

74. Leung VY, Shen J, Wong VW, Jill Abrigo, Grace Lai hung Wong, et al. (2013) Quantitative elastography of liver fibrosis and spleen stiffness in chronic hepatitis B carriers: comparison of shear-wave elastography and transient elastography with liver biopsy correlation. Radiology 269(3): 910-918.

75. Lomonaco R, Godinez Leiva E, Bril F, Sulav Shrestha, Lydia Mansour, et al. (2021) Advanced liver fibrosis is common in patients with type 2 diabetes followed in the outpatient setting: the need for systematic screening. Diabetes Care 44(2): 399-406.

76. Wong VW, Wong GL, Yeung DK, Tina Kit Ting Lau, Carmen Ka Man Chan, et al. (2015) Incidence of non-alcoholic fatty liver disease in Hong Kong: a population study with paired proton-magnetic resonance spectroscopy. J Hepatol 62(1): 182-189.

77. Ferraioli G, Wong VW, Castera L, Annalisa Berzigotti, Ioan Sporea, et al. (2018) Liver ultrasound elastography: an update to the world federation for ultrasound in medicine and biology guidelines and recommendations. Ultrasound Med Biol 44(12): 2419-2440.

78. Loomba R, Quehenberger O, Armando A, Dennis EA (2015) Polyunsaturated fatty acid metabolites as novel lipidomic biomarkers for noninvasive diagnosis of nonalcoholic steatohepatitis. J Lipid Res 56(1): 185-192.

79. Caussy C, Tripathi A, Humphrey G, Shirin Bassirian, Seema Singh, et al. (2019) A gut microbiome signature for cirrhosis due to nonalcoholic fatty liver disease. Nat Commun 10(1): 1406.

80. Govaere O, Cockell S, Tiniakos D, Rachel Queen, Ramy Younes, et al. (2020) Transcriptomic profiling across the nonalcoholic fatty liver disease spectrum reveals gene signatures for steatohepatitis and fibrosis. Sci Transl Med 12(572): eaba4448.

81. Kim D, Kim WR, Kim HJ, Therneau TM (2013) Association between noninvasive fibrosis markers and mortality among adults with nonalcoholic fatty liver disease in the United States. Hepatology 57(4): 1357-1365.

82. Taylor RS, Taylor RJ, Bayliss S, Hannes Hagström, Patrik Nasr, et al. (2020) Association between fibrosis stage and outcomes of patients with nonalcoholic fatty liver disease: a systematic review and meta-analysis. Gastroenterology 158(6): 1611-1625.e12.

83. Park CC, Nguyen P, Hernandez C, Ricki Bettencourt, Kimberly Ramirez, et al. (2017) Magnetic resonance elastography vs transient elastography in detection of fibrosis and noninvasive measurement of steatosis in patients with biopsy-proven nonalcoholic fatty liver disease. Gastroenterology 152(3): 598-607.e2.

84. Katsagoni CN, Georgoulis M, Papatheodoridis GV, Panagiotakos DB, Kontogianni MD (2017) Effects of lifestyle interventions on clinical characteristics of patients with non-alcoholic fatty liver disease: a meta-analysis. Metabolism 68: 119-132.

85. Hannah WN Jr, Harrison SA (2016) Lifestyle and dietary interventions in the management of nonalcoholic fatty liver disease. Dig Dis Sci 61(5): 1365-1374.

86. Wood GC, Chu X, Argyropoulos G, Peter Benotti, David Rolston, et al. (2017) A multi-component classifier for nonalcoholic fatty liver disease (NAFLD) based on genomic, proteomic, and phenomic data domains. Sci Rep 7(1): 43238.

87. Anderson EL, Howe LD, Jones HE, Higgins JP, Lawlor DA, et al. (2015) The prevalence of non-alcoholic fatty liver disease in children and adolescents: a systematic review and meta-analysis. PLoS One 10(10): e0140908.

88. Vos MB, Abrams SH, Barlow SE, Sonia Caprio, Stephen R Daniels, et al. (2017) NASPGHAN clinical practice guideline for the diagnosis and treatment of nonalcoholic fatty liver disease in children: recommendations from the Expert Committee on NAFLD (ECON) and the North American Society of Pediatric Gastroenterology, Hepatology and Nutrition (NASPGHAN). J Pediatr Gastroenterol Nutr 64(2): 319-334.

89. Lassailly G, Caiazzo R, Ntandja Wandji LC, Viviane Gnemmi, Gregory Baud, et al. (2020) Bariatric surgery provides long-term resolution of

nonalcoholic steatohepatitis and regression of fibrosis. Gastroenterology 159(4): 1290-1301.e5.

90. Armstrong MJ, Gaunt P, Aithal GP, Darren Barton, Diana Hull, et al. (2016) Liraglutide safety and efficacy in patients with non-alcoholic steatohepatitis (LEAN): a multicentre, double-blind, randomised, placebo-controlled phase 2 study. Lancet 387(10019): 679-690.

91. McPherson S, Hardy T, Henderson E, Burt AD, Day CP, et al. (2015) Evidence of NAFLD progression from steatosis to fibrosing-steatohepatitis using paired biopsies: implications for prognosis and clinical management. J Hepatol 62(5): 1148-1155.

92. Crossan C, Tsochatzis EA, Longworth L, Kurinchi Gurusamy, Brian Davidson, et al. (2015) Cost-effectiveness of non-invasive methods for assessment and monitoring of liver fibrosis and cirrhosis in patients with chronic liver disease: systematic review and economic evaluation. Health Technol Assess 19(9): 1-409.

93. Younossi Z, Anstee QM, Marietti M, Timothy Hardy, Linda Henry, et al. (2018) Global burden of NAFLD and NASH: trends, predictions, risk factors and prevention. Nat Rev Gastroenterol Hepatol 15(1): 11-20.

94. Paik JM, Golabi P, Younossi Y, Mishra A, Younossi ZM (2020) Changes in the global burden of chronic liver diseases from 2012 to 2017: the growing impact of NAFLD. Hepatology 72(5): 1605-1616.